# Urea indirect electrooxidation by nickel(III) in alkaline medium: from kinetics and mechanisms to reactor modeling

Guillaume Hopsort[a,*], Laure Latapie[a], Karine Groenen Serrano[a], Karine Loubière[a], Theodore Tzedakis[a,*]

Laboratoire de Génie Chimique, Université de Toulouse, CNRS, INPT, UPS, Toulouse, France

*Corresponding authors:

*Pr*. Theodore Tzedakis, theodore.tzedakis@univ-tlse3.fr

*Ph.D. applicant* Guillaume Hopsort, guillaume.hopsort@univ-tlse3.fr

## Abstract

This paper presents an innovative approach to determine and model the kinetics of the catalytic oxidation of urea in alkaline medium on nickel(III) sites. Firstly, the kinetic law is established by considering two types of active sites, either from a chemically synthesized Ni-based powder or from a massive nickel electrode. Thus, the electrochemical regeneration kinetics of nickel(III) can be differentiated from the kinetics of the purely chemical pathway of NiOOH solid particles consumption by urea. Secondly, a mechanism for the urea indirect oxidation mediated by the nickel(III)/nickel(II) system is proposed to predict the formation of all the by-products, contained in the liquid phase that have been experimentally identified in our previous work. Finally, a model combining kinetic laws with diffusive and convective transport phenomena is constructed. The robustness and relevance of the latter are proven by comparing the experimental results obtained during laboratory-scale electrolyzes with those predicted by the model.

## Topical heading & Keywords

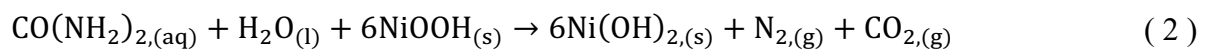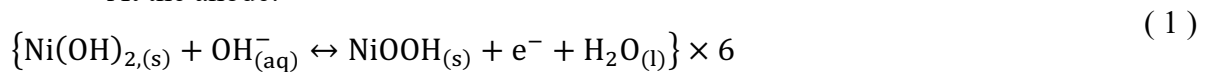'Reaction Engineering, Kinetics and Catalysis'

Urea electro-oxidation; Ni$^{(III)}$/Ni$^{(II)}$ mediator; Mechanism and kinetics; Heterogeneous coupled reactions; Transport phenomena modeling
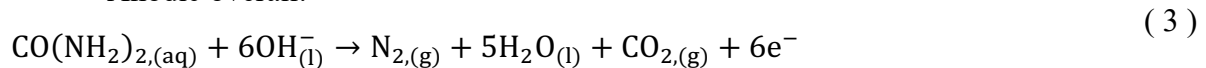
# 1    Introduction

Wastewater treatment and energy issues are nowadays major societal problems requiring numerous investments. Previously considered as a waste, fresh water contaminated by the human activity (intensive breeding, carbon industry, transportation, etc) and by the primary sector is now recognized as a significant source of pollutants valorization. This interest is enhanced as its production is expected to increase by about 50 % by the year 2050[1]. As containing urea (40 %$wt.$[2], at around 0.33 mol.L$^{-1}$), urine constitutes an important source of nitrogen, accounting for nearly 75 % of the nitrogen in watercourses[3]. The urea electrochemical oxidation is nowadays studied for meeting various targets, such as electrolyzers[4–7] (producing H$_2$ as energy carrier), energy production by urea fuel cells[8–13], or advanced electrode materials development[14–17]. Recent investigations[18,19] have claimed that low-cost electrode materials could be used in alkaline media for efficient urea electro-oxidation (UEO), thus opening promising perspectives for UEO implementation at industrial scale. In particular, nickel oxides exhibit important catalytic activity regarding urea oxidation in presence of hydroxide ions, leading to propose a simplified reaction scheme[20–22] described by the Eqs ( 1 )-( 5 ).
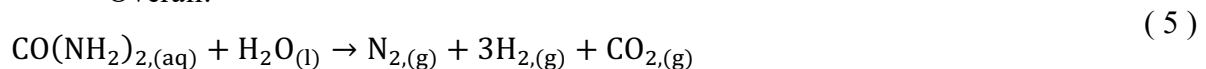
- At the anode:

$$\{Ni(OH)_{2,(s)} + OH^-_{(aq)} \leftrightarrow NiOOH_{(s)} + e^- + H_2O_{(l)}\} \times 6 \tag{1}$$

$$CO(NH_2)_{2,(aq)} + H_2O_{(l)} + 6NiOOH_{(s)} \rightarrow 6Ni(OH)_{2,(s)} + N_{2,(g)} + CO_{2,(g)} \tag{2}$$

- Anodic overall:

$$CO(NH_2)_{2,(aq)} + 6OH^-_{(l)} \rightarrow N_{2,(g)} + 5H_2O_{(l)} + CO_{2,(g)} + 6e^- \tag{3}$$

- At the cathode:

$$6H_2O_{(l)} + 6e^- \rightarrow 3H_{2,(g)} + 6OH^-_{(aq)} \tag{4}$$

- Overall:

$$CO(NH_2)_{2,(aq)} + H_2O_{(l)} \rightarrow N_{2,(g)} + 3H_{2,(g)} + CO_{2,(g)} \tag{5}$$

The redox system NiOOH/Ni(OH)$_2$ acts as a redox mediator catalyzing the urea mineralization. In such a system, the nickel peroxide, NiOOH, is constantly regenerated at the electrode surface by an electrochemical reaction (ER, Eq. ( 1 )). Six electrons, supplied by 6 NiOOH, are required

to achieve a complete mineralization (*i.e.* to convert into $CO_2$ and $N_2$) of one urea molecule according to a heterocatalytic chemical reaction (HCR, Eq. ( 2 )). However, recent works have provided new insights on the urea oxidation by demonstrating that, beyond the formation of $N_2$, various by-products are produced, such as cyanate, nitrite, ammonium and carbonate ions[23,24]. A deeper knowledge of the reaction scheme coupled to the determination of the kinetic law and the related parameters remain a prerequisite to design and to operate UEO processes at industrial-scale. To the best of our knowledge, only two studies are devoted to these investigations. By neglecting the catalytic regeneration of the couple $NiOOH/Ni(OH)_2$ and using Tafel plots, Vedharathinam et al.[25] were the first to propose the following simplified kinetic law as in Eq. ( 6 ) without determining the kinetic constant k.

$$rate_{urea} = k \times [CO(NH_2)_2]^{0.3} \times [OH^-]^2 \qquad (6)$$

Later, partial orders of 1.22 and 0.26 for hydroxide ions and urea respectively on β-NiOOH covered electrode were obtained using cyclic voltammetry and Tafel plots by Singh et al.[26]. The authors have claimed that: *(i)* the reaction order of urea concentration is independent of the applied potential and *(ii)* increasing the applied potential causes the reaction order of the hydroxide ions to decrease. However, in these studies, experiments were carried out in transient state conditions (*i.e.* high potential scan rate $\nu_{scan}$), in which that nickel(III) was not constantly regenerated at the electrode surface, as pointed out in our previous study[27]. As obtained in the mixed ER/HCR regime and at low urea conversion, these related values of reaction partial orders did not allow neither to understand the impact that the secondary reactions occurring at higher urea conversion rates may have on the electrochemical system, nor to get access to relevant intrinsic kinetic information.

To fill this gap, this paper aims at investigating the kinetics of NiOOH catalytic urea oxidation in an alkaline medium. For this purpose, and since neither complete rate law nor kinetic model are described in the literature, a novel approach will be suggested, combining studies of the urea action according to specifically synthesized NiOOH powder and to electrochemically

generated NiOOH sites carried out under steady state conditions. By implementing the catalytic urea oxidation in a suspension of NiOOH solid particles, one can expect to bring new insights on the reaction kinetics by comparing physico-chemical phenomena taking place in the presence of *(i)* non-regenerated NiOOH sites (adsorption, HCR, desorption) on solid particles or *(ii)* electrogenerated NiOOH sites (HCR/ER coupling). Results on the oxidation kinetics with the synthesized nickel particles will be first studied. The experiments performed in a lab-scale electrolysis cell at low scan rates will then enable to determine the key parameters of the kinetic law for the UEO reaction. Furthermore, by combining the newly-established kinetic rate law with the electrolysis results obtained at high urea conversion rates, a detailed mechanism of urea oxidation in alkaline medium on nickel(III) active sites will be proposed, allowing to describe the formation of the liquid phase by-products identified by Tatarchuk et al.[24] and also in our previous work[27].

Section 2 will describe *(i)* the synthesis pathway of the NiOOH powder and the associated characterization techniques, *(ii)* the set-up and the analytical technique to monitor the reaction between urea and nickel(III) particles and, *(iii)* the electrochemical set-up. Section 3 will discuss the kinetic parameters deduced from both chemically and electrochemically synthesized nickel(III) particles, and then elucidate the UEO mechanism. Finally, section 4 will be devoted to the construction of a model able to predict the temporal variation of urea conversion during batch electrolysis and to its validation by comparison with experimental data.


## 2   Experimental

Details concerning chemicals (Normapur® grade) are reported in §SM. 1, see Table SM1.

## 2.1 NiOOH catalyst powder

### 2.1.1 Synthesis

The NiOOH powder was synthesized following the protocols developed by Pan et al.[28] and Thimmasandra et al.[29]. It consisted of oxidizing a $Ni(OH)_2$ powder at room temperature in presence of sodium hypochlorite NaOCl and sodium hydroxide NaOH, as Eq. ( 7 ) below.

$$Ni(OH)_{2,(s)} + OCl^-_{(aq)} \rightarrow NiOOH_{(s)} + \frac{1}{2}Cl_{2,(g)} + OH^-_{(aq)} \qquad (7)$$
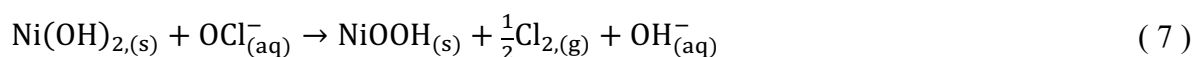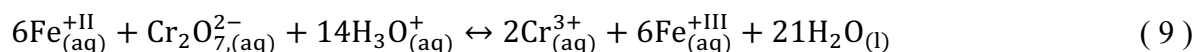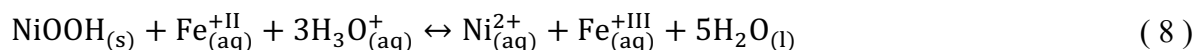
Specifically, NiOOH particles were prepared by mixing 5 g of a commercially available nickel powder (see §SM. 1) with a solution containing 400 mL of sodium hypochlorite and 2 g of sodium hydroxide. The reaction was achieved after 4 hours of magnetic stirring and the mixture obtained was filtered using a Büchner sintered glass filter, and then washed with 6×60 mL of deionized water. The NiOOH powder was finally dried in oven at 80°C during three days.

Using two different concentrations of hypochlorite ($1.76 \times 10^{-1}$ mol.L$^{-1}$ and $7.68 \times 10^{-1}$ mol.L$^{-1}$) powders called Sample 1 and Sample 2 respectively were synthesized to vary the nickel(III) purity.

### 2.1.2 Characterization

Various techniques were used to characterize the initial and the synthesized powders. For sake of clarity, all the results obtained from these methods are reported in the §SM. 2.

Firstly, the purity of the nickel(III) particles was quantified by potentiometric back titration using Mohr's salt. An excess of ferrous salt was introduced into a suspension of NiOOH/Ni(OH)$_2$ particles. After reaction, the excess of ferrous salt was titrated by an acidic solution of potassium dichromate in accordance with Eqs. ( 8 )-( 9 ).

$$NiOOH_{(s)} + Fe^{+II}_{(aq)} + 3H_3O^+_{(aq)} \leftrightarrow Ni^{2+}_{(aq)} + Fe^{+III}_{(aq)} + 5H_2O_{(l)} \tag{8}$$

$$6Fe^{+II}_{(aq)} + Cr_2O^{2-}_{7,(aq)} + 14H_3O^+_{(aq)} \leftrightarrow 2Cr^{3+}_{(aq)} + 6Fe^{+III}_{(aq)} + 21H_2O_{(l)} \tag{9}$$

The purity was determined as the ratio of the mass of nickel(III) deduced from the titration to the initial mass of the $Ni(OH)_2$ powder used in the trial. The set-up related to these experiments is schematically described in Figure SM2.

The crystalline structure of the nickel synthesized powders was studied by XRD analysis using a diffractometer (MiniFlex600 - D/Tex Ultra2, Rigaku®, Japan) with Cu-Kα radiation (40 kV, 15 mA). Data, illustrated in Figure SM4, were collected in the 2θ range of 5-92°. The step width was 0.02° with a scan speed of 10°.min$^{-1}$. From the literature on nickel(III) XRD characterizations[29–33], the initial powder was well identified as nickel(II) hydroxide β-$Ni(OH)_2$ with a brucite-type structure. After synthesis, samples 1 and 2 were founded to be nickel(III) as β-NiOOH according to diffraction peaks for (001) and (002) crystal faces at 19 and 37° [34]. It is noted that the peaks associated with $Ni(OH)_2$ have disappeared. The differences in peak intensities between spectra 2 and 3 could be explained by some differences in crystallinity (a slight amorphous phase could be present in sample 2) which could broaden the diffraction peaks.

Scanning Electron Microscopy (SEM) images were obtained using a microscope (JSM 7100F, JEOL®, Benelux) operated at 10 kV. As shown in Figure SM5, the morphology of the various particles did not significantly change after the reaction with hypochlorite and the resulting particles could be assumed as spherical in shape with a wide size distribution from 1 to 30 μm. These particles, or at least the shell around the particle, are supposed to be composed by NiOOH sites.

A laser diffraction particle size analyzer (Mastersizer MS3000, Malvern Instruments®, United-Kingdom) was used to determine the particle size distributions in terms of number and volume. The characteristic diameters of the number and volume distributions of the initial and synthesized powders are reported in Table 1.

Relative densities of the nickel particles were measured via a helium pycnometer (AccuPyc 1330, Micromeritics®, United States). They underwent minor modifications both before and after the synthesis (see Table 1).

BET measurements (BELSORP-mini II, BEL®, Japan) were made to quantify the porosity and specific area of the particles. As the synthesis reaction of nickel(III) particles consisted in exchanging an electron and a proton, the properties of the particles (porosity, pore diameter, particle size) were slightly modified before and after synthesis. Table 1 summarizes all the physical properties of the initial nickel(II) powder and of the synthesized nickel(III) powders.

Table 1 Physical properties of the initial nickel(II) powder and of the nickel(III) powders

| | Purity of nickel(III) content (%) | Density $(g.cm^{-3})$ | Particle size analysis (µm) | | | | | | | | | | Specific surface area $(m^2.g^{-1})$ | Mean pore diameter (nm) |
| | | | Volume distribution | | | | | Number distribution | | | | | | |
| | | | $d_{10}$ | $d_{50}$ | $d_{90}$ | $d_{32}$ | $d_{43}$ | $d_{10}$ | $d_{50}$ | $d_{90}$ | $d_{32}$ | $d_{43}$ | | |
|---|---|---|---|---|---|---|---|---|---|---|---|---|---|---|
| Initial Ni(II) powder | 0 | $3.7 \pm 0.1$ | 3.9 | 9.0 | 16.9 | 5.4 | 9.8 | 0.4 | 0.5 | 0.8 | 5.5 | 10.0 | $6.67 \pm 0.17$ | $8.2 \pm 0.1$ |
| Ni(III) powder – Sample 1 | $79 \pm 2$ | $3.9 \pm 0.1$ | 5.5 | 12.3 | 24.0 | 9.9 | 13.7 | 1.3 | 3.4 | 8.1 | 9.9 | 13.7 | | |
| Ni(III) powder – Sample 2 | $29 \pm 2$ | $3.8 \pm 0.1$ | 4.5 | 10.0 | 20.5 | 7.9 | 11.4 | 0.7 | 1.3 | 5.3 | 7.9 | 11.4 | $8.51 \pm 0.12$ | $7.7 \pm 0.1$ |

### 2.2 Kinetics investigations of the reaction between urea and chemically synthesized nickel(III) sites in alkaline medium

#### 2.2.1 Experimental set-up and reaction monitoring

The experimental set-up used to monitor the catalytic oxidation of urea by nickel(III) particles in alkaline medium, consisted of a closed double-walled thermoregulated reactor operating under nitrogen atmosphere (nitrogen was previously humidified to avoid any decrease of the reaction volume) (illustrated §SM. 3, see Figure SM6). The reactor initially contained a suspension of 5 g of synthesized powder into 45 mL volume of KOH solution at different concentrations. Ultrapure water 18.2 MΩ.cm was systematically used to prepare suspensions.

A strong stirring created by a suitable magnetic bar ($\frac{\phi_{reactor}}{\phi_{magnetic\ bar}} = \frac{6.5}{4.8}$, 800 RPM) ensured that all of the particles were thoroughly suspended. Before introducing urea, the suspension containing NiOOH/Ni(OH)$_2$ particles was stirred during 5 min in order to finely disperse the nickel powder into the whole KOH volume. The aqueous deaerated alkaline solution of urea was then injected with a syringe through a septum. Each experiment was performed twice to ensure repeatability.

The consumption of hydroxide ions was monitored via the pH to study the reaction kinetics. To succeeds, this method required a precise pH meter (3 digits), a calibration at the appropriated pH range (pH 13-14), and a glass electrode resistant to the involved suspension. To fill these conditions, a Metrohm® Unitrode electrode was used enabling to record the pH every 0.5 second with an accuracy of ± 0.001 pH units. Typical examples of the temporal variation of pH recorded in this study are shown in Figure SM7. One could observe that, at the beginning of the recording, a transitional stage occurred corresponding to the time required to reach the perfectly mixed state of the liquid-solid suspension, before injecting the urea alkaline solution (5 mL). The two curves plotted on this figure also highlighted the satisfactory repeatability of the experiments when two different solutions of urea in hydroxide solutions were injected in two identical suspensions of nickel(III) particles.

To understand how the reagent concentrations could affect the oxidation kinetic, and subsequently to identify the relevant kinetic parameters, an experimental workplan was established. It allowed varying the hydroxide concentrations from $5 \times 10^{-3}$ to $5 \times 10^{-2}$ mol.L$^{-1}$ and the urea concentrations from $10^{-2}$ to $3 \times 10^{-1}$ mol.L$^{-1}$ (note that the latter value corresponded to the order of magnitude of the urea concentration in human urine). In addition, the nickel(III) concentration was modified by working with both powders of nickel(III) of different purities.

As a preliminary step, it was verified that *(i)* the chemical reaction occurring when an alkaline urea solution was put into contact with chemically synthesized nickel(III) particles led to

identical by-products in the liquid phase when compared to the ones taking place on nickel bare electrode, and *(ii)* the total organic carbon (TOC) concentration decreased during the reaction course. For this purpose, the analytical procedure established in our previous study[27] was used, involving ionic chromatography and non-purgeable organic carbon.

### 2.2.2 *Post-processing of the temporal pH-curves*

The instantaneous rate of the reaction described by Eq. ( 2 ), expressed in $mol. (m^3. g_{cat}. s)^{-1}$ and noted $r_\chi$, was defined as the derivative of the extent of reaction, $\xi$, with respect of time, as shown in Eq. ( 10 ).

$$r_\chi = -\frac{1}{m_{cat} \times V}\frac{d\xi}{dt} = -\frac{1}{m_{cat} \times V}\frac{dn_{CO(NH_2)_2}}{dt} = -\frac{1}{m_{cat} \times V \times \nu_{Ni(III)}}\frac{dn_{Ni(III)}}{dt}$$
$$= -\frac{1}{m_{cat} \times \nu_{OH^-}}\frac{d[OH^-]}{dt}$$
( 10 )

where $m_{cat}$ is the nickel(III) mass (expressed in grams of catalyst, $g_{cat}$), $\nu_i$ the stochiometric coefficient of the reactant i in Eq. ( 2 ), $V$ the reaction mixture volume (assuming the volume constant versus time, $m^3$) and $n_{Ni(III)}$ the amount of nickel(III) sites into the solid particles of NiOOH/Ni(OH)$_2$ that were accessible to the reagents (urea and OH$^-$).

The kinetic law of the chemical reaction was assumed to obey to Eq. ( 11 ).

$$r_\chi = k_\chi \times [CO(NH_2)_2]^{\alpha_\chi} \times [OH^-]^{\beta_\chi} \times (\rho_{cat})^{\gamma_\chi}$$
( 11 )

where $\alpha_\chi, \beta_\chi, \gamma_\chi$ are the partial orders of the reaction, respectively related to urea, hydroxide, and chemically synthesized nickel(III) sites, $k_\chi$ the reaction rate constant $(mol^{1-(\alpha_\chi+\beta_\chi)}. (m^3)^{\alpha_\chi+\beta_\chi+\gamma_\chi-1}. g_{cat}^{-(1+\gamma_\chi)}. s^{-1})$ and $\rho_{cat}$ the mass concentration of nickel(III) per unit of volume ($g_{cat}.m^{-3}$).

Despite the similarity in terms of by-products, the fundamental mechanisms underlying the urea degradation (in particular the adsorption/desorption ones) were different, depending whether the nickel(III) sites used was electrochemically generated or chemically synthesized. For this

reason, distinct notations were used for the kinetic law: $r_\chi$ for chemically synthesized sites (defined in Eq. ( 11 )) and $r_{E\chi}$ for electrogenerated sites.

The conversion rate of the HCR reaction, noted $X$, could be calculated from the pH measurements, according to Eq. ( 12 ).

$$X(t) = 1 - \frac{10^{pH_{(t)}-14}}{10^{pH_{t=0}-14}} \qquad (\,12\,)$$

The experimental curves, $pH_{(t)}$, were systematically smoothed using a polynomial of order 6 as the raw data were slightly noisy, mainly due to disturbances caused by the stirring and specifically by the flow of the solid particles across the pH electrode.

In this work, the initial reaction rates, $r_\chi^0$, were determined for conversions never exceeding 5 % of the initial hydroxide concentration, and calculated from the slope of the $pH_{(t)}$ curve measured some seconds after the urea injection. The time period considered to calculate theses slopes (typically between 5 s and 50 s) slightly impacted the obtained valued, as shown in Table SM2 (see §SM. 4).

## 2.3 Kinetic investigations of the reaction between urea and the electrochemically generated nickel(III) sites in alkaline medium

### 2.3.1 Experimental set-up

The same set-up than the one developed in our previous study[27] was used for determining the partial orders. The three-electrode cell was connected to a potentiostat (PGSTAT 128 N, Metrohm Autolab®, Switzerland), and consisted of:

- a nickel rotating disk (2 mm diameter) as working electrode (WE),
- a Hg/HgO as reference electrode (Origasens, Origalys®, France),
- a Pt foil (40 mm$^2$) as counter-electrode (CE).

All trials were repeated 3 times and the potentials were reported *vs.* Hg/HgO throughout the article. The temperature of the reaction medium was regulated by flowing a thermostatic

solution in the double-jacketed electrochemical cell. Measurements were performed using various concentrations of urea and KOH, and four different working electrode surfaces, ranging from 8.7 to 15.4 mm$^2$. The latter were elaborated by introducing a thin square shaft into a glass tube filled of alkaline resistant glue and then polished to obtain a smooth rectangular section of bare nickel with surface areas mentioned above.

### 2.3.2   Expression of reaction rate

The reaction rate of the HCR on electrogenerated nickel(III) sites, standardized by the electrode surface, was expressed in $\text{mol.}\left(m_{elec}^2.\,m_{bulk}^3.\,s\right)^{-1}$ and defined as the flux density of the superficial chemical reaction by Eq. ( 13 ).

$$r_{E\chi} = k_{E\chi} \times [CO(NH_2)_2]_{(t)}^{\alpha_{E\chi}} \times [OH^-]_{(t)}^{\beta_{E\chi}} \times (S_{elec})^{\gamma_{E\chi}} \qquad (13)$$

where

$k_{E\chi}$ as the reaction rate constant $\left(mol^{1-(\alpha_{E\chi}+\beta_{E\chi})}.\left(m_{elec}^2\right)^{-(1+\gamma_{E\chi})}.\left(m_{bulk}^3\right)^{\alpha_{E\chi}+\beta_{E\chi}-1}.s^{-1}\right)$, $S_{elec}$ the surface of the bare nickel electrode $(m_{elec}^2)$ and $\alpha_{E\chi}, \beta_{E\chi}, \gamma_{E\chi}$ the partial orders of urea, hydroxide, and electrochemically generated nickel(III), respectively.

## 3   Results on the kinetic of the urea catalytic indirect oxidation

### 3.1   Case 1: with chemically synthesized nickel(III) sites

#### 3.1.1   Determination of the initial kinetic rate law

The initial rate method is a well-known approach[35,36], enabling to determine the partial orders of each reactant by varying its concentration while keeping constant the other reactant concentrations and the operating conditions (temperature, stirring).

To determine the partial order of urea, noted $\alpha_\chi$, several temporal pH-measurements are performed and the related initial rates, $r_\chi^0$, determined. By varying the initial concentration of urea between 0.02 and 0.25 mol.L$^{-1}$, and by keeping [OH$^-$] = 0.005 mol.L$^{-1}$ and the nickel

particle mass equal to 30 $kg_{cat}.m^{-3}$ (nickel(III) powder - sample 2), the initial kinetic rate law (Eq. ( 10 )) can be written as the Eq. ( 14 ).

$$r_\chi^0 = k_{app} \times [CO(NH_2)_2]^{\alpha_\chi} \qquad ( 14 )$$

where $k_{app}$ is the related apparent constant ($mol^{1-\alpha_\chi}.(m^3)^{\alpha_\chi-1}.(g_{cat}.s)^{-1}$).
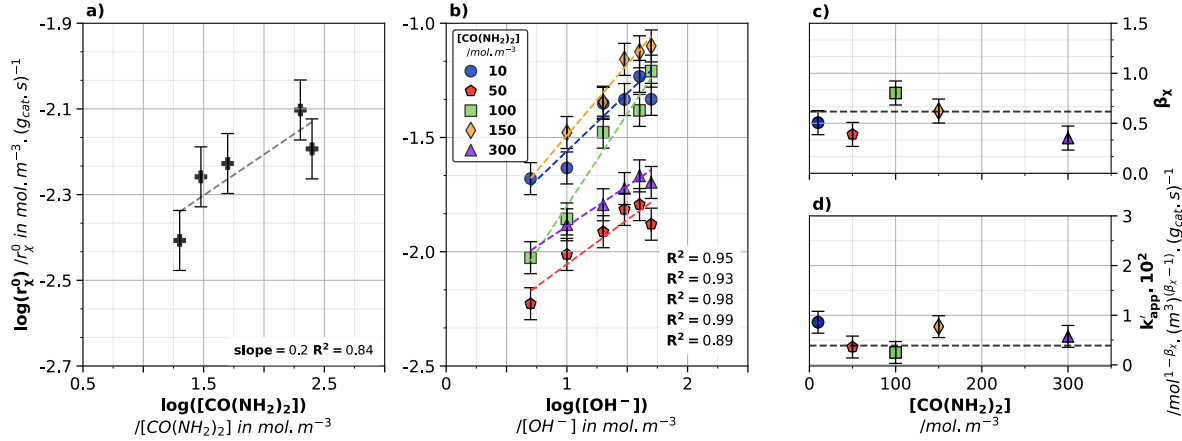


Figure 1 Kinetic experiments with chemically synthesized nickel(III) sites: measurements of the initial rate versus the concentration of a) urea and b) potassium hydroxide. Graph c) provides the values of $\beta_\chi$ as a function of the KOH concentration for different urea concentrations. $k'_{app}$ remains constant whatever the urea concentration, as shown in the graph d). Graph a) was achieved with a 5 $mmol.L^{-1}$ KOH solution. All these results were obtained with nickel(III) synthesized powder – Sample 2.

The variation of the logarithmic initial reaction rate versus the logarithmic urea concentration, plotted in Figure 1-a, can be assumed linear despite a rather strong dispersion. From the slope of the related straight line, the partial order of urea is found equal to $\alpha_\chi = 0.2 \pm 0.1$. This low value suggests that the kinetic rate slightly depends on the urea concentration, which could be explained by several reasons:

(i) the strong affinity of the nickel peroxides particles for the urea. Let's consider that the adsorption of urea on nickel(III) sites obeys to a Langmuir isotherm as shown in Eq. ( 15 ).

$$\Gamma = \frac{\Gamma_{max} \times K \times [CO(NH_2)_2]}{1 + K \times [CO(NH_2)_2]} \qquad ( 15 )$$

where $\Gamma$ the nickel surface concentration ($mol.m^{-2}$), $\Gamma_{max}$ the maximum nickel surface concentration available on nickel oxide particles ($mol.m^{-2}$) and K is the equilibrium constant of the adsorption step.

In this case, the urea superficial concentration on the nickel(III) sites can be simplified $(K \times [CO(NH_2)_2] \gg 1)$ as Eq. ( 16 ).

$$\Gamma = \Gamma_{max} \tag{16}$$

This means that adsorption is rapid and limited by accessible nickel(III) sites. Regardless of the volume concentration of urea, its superficial concentration remains constant and equal to $\Gamma_{max}$, and thus the nickel(III) surface is saturated with urea.

*(ii)* the mass transfer limitations of the reagents into the internal nickel oxides layers of core-shell particles.

The same method was implemented for determining the hydroxide partial order, $\beta_\chi$, by varying the related concentration between 0.005 and 0.05 mol.L$^{-1}$. Here, the simplified initial kinetic rate law can be deduced from Eq. ( 10 ) and can be written as Eq ( 17 ).

$$r_\chi^0 = k'_{app} \times [OH^-]^{\beta_\chi} \tag{17}$$

where $k'_{app}$ is the related apparent constant (as $k'_{app} = k_\chi \times [CO(NH_2)_2]^{0.2} \times (\rho_{cat})^{\gamma_\chi}$).

Figure 1-b presents the variation of the logarithmic initial reaction rate versus the logarithm of the hydroxide concentration, for five different urea concentrations ranging from 0.01 to 0.3 mol.L$^{-1}$. These variations are assumed linear and their slopes, determined for various urea concentrations, are reported in Figure 1-c. This leads to $\beta_\chi = 0.6 \pm 0.2$. As urea has been found to slightly impact the reaction rate, a small variation of the apparent constants, $k'_{app}$, as a function of the urea concentration is observed in the inset of Figure 1-d, likely due to some measurement errors. From this, an average value of the apparent constant is found equal to 0.38 $\times$ 10$^{-2}$ mol$^{0.4}$.(m$^3$)$^{-0.4}$.(g$_{cat}$.s)$^{-1}$.

By modifying the nickel(III) purity of the synthesized powders (Samples 1 and 2, see Table 1) and keeping constant the initial concentrations of urea at 0.3 mol.L$^{-1}$ and of hydroxide at 0.005 mol.L$^{-1}$, the partial order of nickel(III), $\gamma_\chi$, can be deduced as Eq. ( 18 ).

$$r_\chi^0 = k_{app}'' \times (\rho_{cat})^{\gamma_\chi} \tag{18}$$

where $k_{app}''$ is the related apparent constant $(mol.\,(m^3)^{\gamma_\chi-1}.\,g_{cat}^{-(1+\gamma_\chi)}.\,s^{-1})$.

Considering that the mass concentration of nickel(III), $\rho_{cat}$, is the product of the mass of powder introduced and the nickel(III) content in the powder, the slope of the Eq. ( 19 ) allows to determine the reaction order of nickel(III).

$$\ln(r_\chi^0) = \ln(k_{app}'') + \gamma_\chi \times \ln\,(\text{mass of powder} \times \text{purity}) \tag{19}$$

At last, $\gamma_\chi$ is found almost equal to $1.9 \pm 0.2$ which can be interpreted as the number of nickel(III) sites (NiOOH in fact) involved in the urea oxidation reaction.

Once the partial orders are determined, the kinetic constant, $k_\chi$, is calculated using the values of *(i)* initial concentrations of the reagents and of *(ii)* initial rates measured for 35 trials according to Eq. ( 11 ). As illustrated in Figure SM8 (see §SM. 5), $k_\chi$ is ranging from $k_{\chi,low} = 0.24 \times 10^{-12}$ to $k_{\chi,high} = 7.7 \times 10^{-12}\,mol^{0.2}.\,(m^3)^{1.7}.\,g_{cat}^{-2.9}.\,s^{-1}$, the average value being equal to is $k_{\chi,mean} = 3.8 \times 10^{-12}\,mol^{0.2}.\,(m^3)^{1.7}.\,g_{cat}^{-2.9}.\,s^{-1}$.

Therefore, the overall empirical kinetic law of urea oxidation in presence of chemically generated nickel(III) sites can be expressed by Eq. ( 20 ).

$$r_\chi = (3.8 \pm 2.0) \times 10^{-12} \times [CO(NH_2)_2]^{0.2} \times [OH^-]^{0.6} \times \rho_{cat}^{1.9} \tag{20}$$

It should be kept in mind that *(i)* as the urea molecules penetrate into the NiOOH/Ni(OH)$_2$ particles, they are oxidized and the NiOOH is reduced to Ni(OH)$_2$ and *(ii)* the urea oxidation products generated have then to diffuse deeper into the particle to encounter another nickel(III) active site and to continue their mineralization. As mentioned above, the occurrence of mass transfer limitations could also contribute to slow down the reaction rate.

In the case of such synthesized nickel particles, the regeneration of nickel(III) sites cannot occur after being consumed by urea, which will inevitably modify the rate law here obtained.

### 3.1.2 Validation of the initial kinetic rate law by the integral method

In this section, it is assumed that there is no limitation by the mass transport (urea or/and OH⁻), inside or outside of the $NiOOH/Ni(OH)_2$ particles. Following this assumption, the validity of the kinetic rate law determined previously (Eq. ( 20 )) must be confirmed. To this end, it is necessary to numerically integrate the equation as a function of time and to confront the theoretical temporal evolutions of the reactant concentrations with the experimental data.

Using the integral method for kinetic investigations offers the advantage[37] to validate the reaction orders and the rate constant obtained using the initial rate method (*i.e.* at short times and very low OH⁻ conversions below 5 %) for longer periods where high conversions are achieved and where secondary reactions can also occur. The method for doing so entails a comparison between the experimental and predicted temporal variations in OH⁻ concentration in order to validate the law derived from initial kinetics.

Table 2 presents the chemical amounts of reactants, initially and at any time, where X represents the hydroxide conversion rate.

Table 2 Extent of urea oxidation reaction by chemically synthesized nickel(III) sites where V represents the liquid reaction volume ($4.5 \times 10^{-5}$ m³), $m_{cat}$ the mass of powder (5 g), $M_{NiOOH}$ the NiOOH molar mass (91.7 g.mol⁻¹) and X the conversion in hydroxide ions.
The corresponding overall reaction is written as $CO(NH_2)_2 + 6OH^- + 6Ni^{+III} \rightarrow$ products

|  | moles of CO(NH₂)₂ | moles of OH⁻ | moles of NiOOH | moles of accessible NiOOH |
|---|---|---|---|---|
| t=0 | $a = [CO(NH_2)_2]°V$ | $b = [OH^-]°V$ | $c = \dfrac{m_{cat}}{M_{NiOOH}} \times$ purity | $c' = c \times \varepsilon$ |
| t | $a - \dfrac{bX}{6}$ | $b(1-X)$ | $c - bX$ | $c' - bX$ |

Without considering the real accessibility of the nickel(III) sites in the synthesized core-shell particles, the theoretical profiles tend towards the experimental values but significant deviations of magnitude are obtained (deviation > 50 %) and even more for the highest reactant concentration (results not shown). In order to describe the physics of the system (*i.e.* spherical layers of NiOOH around a core of Ni(OH)₂), a surface accessibility factor of nickel(III), noted

ε, is voluntarily introduced. Such choice is motivated by the fact that *(i)* the spatial distribution of nickel(III) on solid particles is probably not uniform, and *(ii)* the oxidation reaction of urea on nickel particles is a surface reaction, and the by-products and reaction intermediates formed inside the particle are consuming the OH⁻ ions. This latter consumption, not considered in the kinetic model here studied, will lead to a diffusional limitation of hydroxide ions within the particles. The parameter, ε, offers the advantage to fill this bias. Note that the relating value, not measured, will be the single fitting parameter of the model.

By coupling Eq. ( 10 ) expressed as a function of hydroxide ions and Eq. ( 20 ), it comes Eq. ( 21 ).

$$\frac{dX}{dt} = \frac{6 m_{cat} k_\chi b^{0.6}}{[OH^-]^0} \times \left(\frac{6a - bX}{6V}\right)^{0.2} \times \left(\frac{(1 - X)}{V}\right)^{0.6} \times \left(\frac{(c' - bX) \times M_{NiOOH}}{V}\right)^{1.9} \qquad ( 21 )$$

The previous equation is numerically solved (using scipy.integrate.odeint Python package solving a system of ordinary differential equations), and the theoretical temporal conversion of hydroxide with time is obtained, as reported in Figure 2. The surface accessibility factor of nickel(III), ε, used to plot these figures is equal to 2.6 %, suggesting then that a small amount of nickel(III) is available for the chemical reaction. Indeed, after a first cycle of adsorption onto the powder, the urea molecules having a strong affinity to nickel(III) could induce a "screen effect", thus reducing the number of nickel(III) sites into the internal layers of the particles. Figure 2 also reports a sensitivity study with respect to the chemical kinetic constant, $k_\chi$: a maximum deviation of 20 % is observed for the reaction times longer than 600 seconds. The validity of the kinetic rate law is then checked by considering several initial concentrations of urea and hydroxide ions. Whatever the concentrations, the numerical profiles of the conversion of OH⁻ do not deviate (maximum deviation of 6 %) from the experimental data for X < 20 % (ε = 2.6 %). As expected, higher conversions are observed when the initial hydroxide ions concentration is decreased.

Figure 2 shows that the temporal profiles obtained using the kinetic rate law constant $k_{\chi,low}$, $k_{\chi,mean}$ or $k_{\chi,high}$ determined from the previous section (see §SM. 5) are in very good agreement (maximum deviations of 10 %) with the experimental ones for a period longer than 200 sec. It can be noted that for unfavorable conditions, illustrated in Figure 2-c (*i.e.* the lowest ratio between initial concentration of hydroxide ions and urea, almost equal to $1.7 \times 10^{-2}$), the deviation between the experimental and predictive profiles is higher than 20 % after 600 sec. This slowing down of the urea oxidation could be explained in several ways: *(i)* an internal diffusional limitation of the reactants (urea and hydroxide) and by-products in the particles could limit the reaction process after consuming all the nickel(III) active sites on the catalyst surface and *(ii)* a competitive adsorption between the by-products and the reactants could also occur.
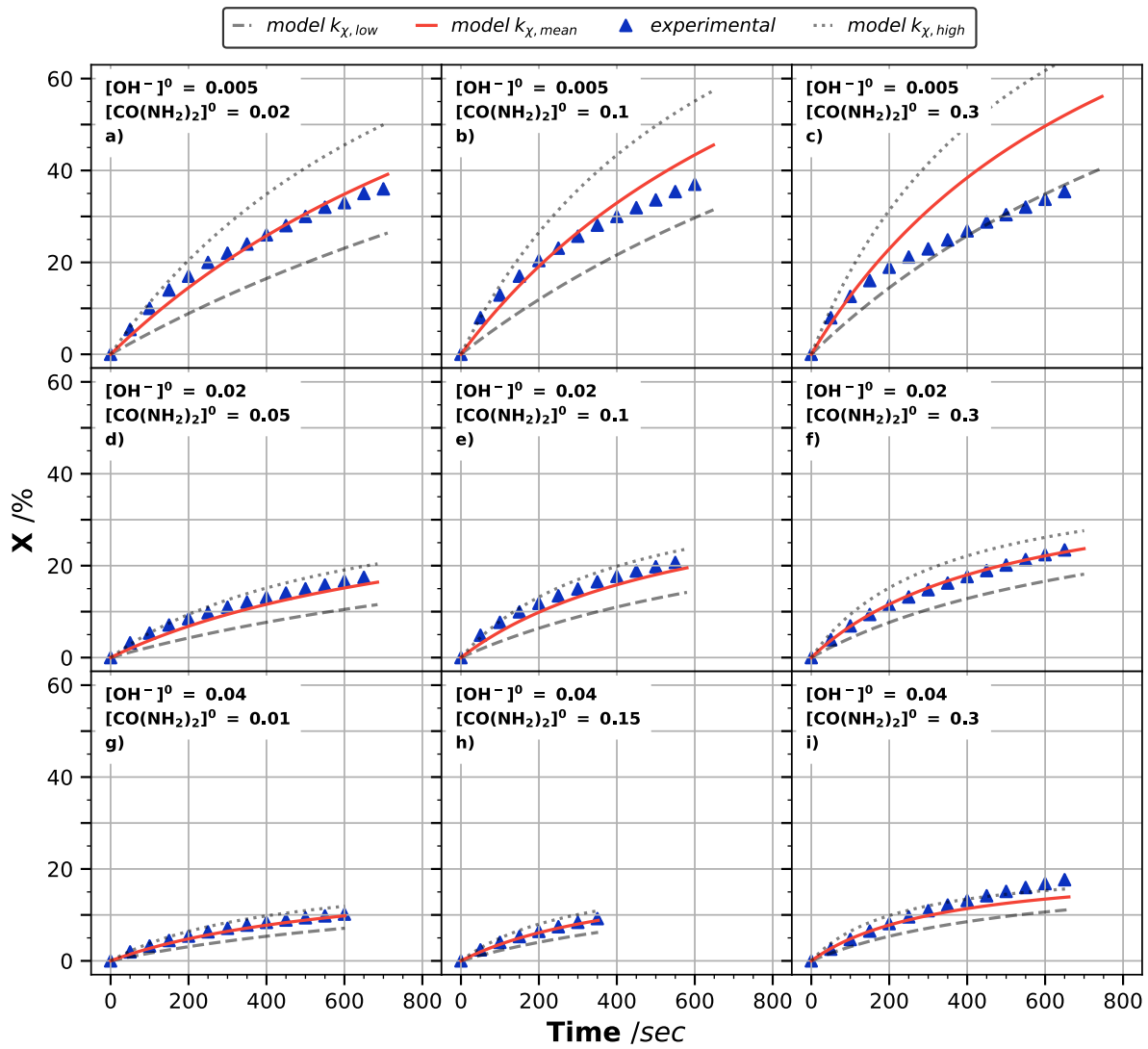
Figure 2 Comparison of the experimental temporal evolutions of the hydroxide ion conversion to the ones obtained by numerical solving of the Eq. ( 21 ) for different initial concentrations of urea and hydroxide (molar concentration are expressed in mol.L$^{-1}$). The surface accessibility factor of nickel(III), ε, is equal to 2.6 % whatever the graphs.

### 3.2 Case 2: with the electrochemically synthesized nickel(III) sites on bare nickel electrode

In the present section, the NiOOH sites are electrochemically regenerated on a bare nickel anode and react with urea. As shown in our previous work[27], the coupling of the HCR (Urea/NiOOH) with the ER (NiOOH/Ni(OH)$_2$) allows to continuously regenerate the active nickel(III) sites if the nickel oxides anode is polarized to the appropriated potential. It becomes then possible to study only the HCR and thus to avoid the adsorption/desorption processes as well as the mass transport of urea and oxidation products from one nickel(III) molecule to the

other (see §3.1.2). For that, the current potential curves have been plotted by applying a potential scan rate lower than 1 mV.s⁻¹. This technique has been here applied for different operating parameters, with the aim of establishing the kinetic law of the UEO in presence of electrogenerated NiOOH sites at the anode.

The i-E curves obtained at steady state conditions are showed in Figure 3-a-b-c. From them, the partial orders of urea, hydroxide ions and nickel(III) sites has been determined, as shown in Figure 3-d-e-f respectively.
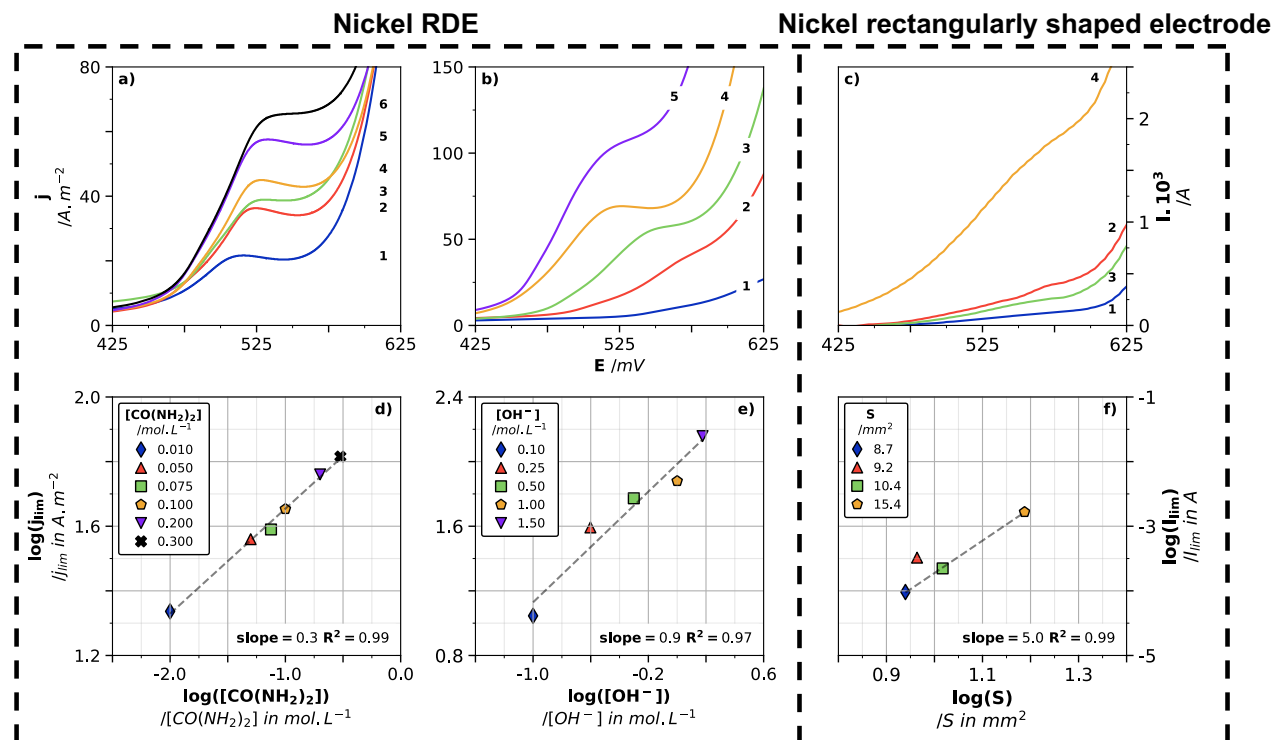


Figure 3 Kinetic experiments with electrochemically synthesized nickel(III) sites on bare nickel electrode.
*Top*: Graphs a), b) and c) present j/I-E curves obtained at the steady state (0.12 mV.s⁻¹) using a Ni WE immersed in 100 mL of alkaline solutions of urea, thermoregulated at 298 K.
Graph a) effect of urea concentration on the shape of the i-E curves obtained on nickel RDE in alkaline solution of KOH (1 mol.L⁻¹) at 1000 RPM with urea concentrations at 0.01 mol.L⁻¹ (1), 0.05 mol.L⁻¹ (2), 0.075 mol.L⁻¹ (3), 0.1 mol.L⁻¹ (4), 0.2 mol.L⁻¹ (5) and 0.3 mol.L⁻¹ (6).
Graph b) effect of KOH concentration on the shape of the i-E curves obtained on nickel RDE in urea solution of 0.3 mol.L⁻¹ stirred at 1000 RPM with hydroxide concentrations at 0.1 mol.L⁻¹ (1), 0.25 mol.L⁻¹ (2), 0.5 mol.L⁻¹ (3), 1 mol.L⁻¹ (4) and 1.5 mol.L⁻¹ (5).
Graph c) effect of the geometric surface area (rectangularly area) of the nickel electrode on the shape of the i-E curves obtained with an urea concentration of 0.3 mol.L⁻¹ and a KOH concentration of 1 mol.L⁻¹, using geometrical electrode surfaces equal to 8.7 mm² (1), 9.2 mm² (2), 10.4 mm² (3) and 15.4 mm² (4).
*Bottom*: The partial orders of urea ($\alpha_{E,\chi}$), hydroxide ions ($\beta_{E,\chi}$) and nickel(III) ($\gamma_{E,\chi}$) were determined from the curves respectively plotted in Figures d), e) and f), deduced from the logarithm plot of the limiting current magnitude (at the diffusion limitation area) as a function of the logarithmic reactant concentration.

The potentiostatic polarization of the nickel electrode at the plateau of the i-E curves allows the anode to be covered by Ni(OH)$_2$ which oxidizes into NiOOH. The urea is oxidized by chemical reaction with NiOOH which is reduced into the Ni(OH)$_2$, immediately oxidized on the nickel electrode into NiOOH, thus releasing its electron. The newly regenerated NiOOH goes on a new cycle with the urea oxidation intermediate, thus meaning that the urea and its intermediates formed could be oxidized by the same nickel system, without any mass transfer limitation. The oxidation process continues until obtaining the final products (N$_2$, CO$_2$, etc).

Under steady state conditions, the mass balance on nickel(III) is expressed as the Eq. ( 22 ).

$$\frac{d\Gamma_{III}}{dt} = \frac{I_{plateau}}{n\mathcal{F}S_{electrode}} - \nu_{Ni^{III}} \times r_{E\chi} \times V \tag{22}$$

where $\Gamma_{III}$ is the nickel surface concentration (mol.m$^{-2}$), $I_{plateau}$ as the limiting current, observed at the plateau signal (A), n the number of exchanged electron (1, dimensionless), $\mathcal{F}$ the Faraday constant (C.mol$^{-1}$), $\nu_{Ni^{III}}$ the stochiometric coefficient of nickel(III) and $r_{E\chi}$ the reaction rate of the HCR on electrogenerated nickel(III) sites (mol. $\left(m_{elec}^2 . m_{bulk}^3 . s\right)^{-1}$).

It is obvious that after a certain time, the redox system NiOOH/Ni(OH)$_2$ will reach a steady state until the concentration of urea is sufficient to supply the system. In this case, the accumulation of the nickel(III) at the nickel surface can be assumed equal to zero. The current intensity of the plateau is thus proportional to the reaction rate as Eq. ( 23 ).

$$I_{plateau}^{\infty} = n\mathcal{F} \times V \times \nu_{Ni^{III}} \times k_{E\chi} \times [CO(NH_2)_2]^{\alpha_{E\chi}} \times [OH^-]^{\beta_{E\chi}} \times (S_{electrode})^{\gamma_{E\chi}+1} \tag{23}$$

where $I_{plateau}^{\infty}$ is the limiting current in steady state conditions (A).

As for the initial rate method in the §3.1.1, by applying the logarithm to Eq. ( 23 ) and by varying the molar concentration of one reactant, the partial orders can be deduced, according to Eqs. ( 24 )-

( 26 ).

$$\log\left(j_{plateau}^{\infty}\right) = \log\left(n\mathcal{F} \times k_{E\chi} \times [OH^-]^{\beta_{E\chi}} \times (S_{electrode})^{\gamma_{E\chi}}\right) + \alpha_{E\chi} \times \log([CO(NH_2)_2])$$

$$\tag{24}$$

$$\log\left(j_{plateau}^{\infty}\right) = \log\left(n\mathcal{F} \times k_{E\chi} \times [CO(NH_2)_2]^{\alpha_{E\chi}} \times (S_{electrode})^{\gamma_{E\chi}}\right) + \beta_{E\chi} \times \log([OH^-])$$

( 25 )

$$\log\left(I_{plateau}^{\infty}\right) = \log\left(n\mathcal{F}S_{electrode} \times k_{E\chi} \times [CO(NH_2)_2]^{\alpha_{E\chi}} \times [OH^-]^{\beta_{E\chi}}\right) + \gamma_{E\chi} \times \log(S_{electrode})$$

( 26 )

where $j_{plateau}^{\infty}$ is the limiting current density corresponding to the plateau of the signal in steady state ($A.m^{-2}$).

The related plots are reported in Figure 3-d-e-f. A value of $\alpha_{E\chi} = 0.3 \pm 0.1$ is obtained for the partial order of urea, which is in agreement with the value obtained with chemically synthesized nickel(III) sites (see section §3.1.1). The partial order of hydroxide ions is found equal to $\beta_{E\chi} = 0.9 \pm 0.1$. This value is slightly higher than the previously one ($\beta_{\chi} = 0.6$), which can be attributed to the fact that additionally to the urea oxidation, the electrogeneration of nickel(III) requires one hydroxide ion and thus implies a stronger dependence of the chemical rate by hydroxide ions. At last, the partial order of nickel(III) is found equal to $\gamma_{E\chi} = 5.0 \pm 0.5$. This high value would suggest that, during the potentiostatic polarization, a nickel active site is regenerated 5 times on the electrode surface per adsorbed urea. Since the number of urea adsorption sites onto nickel(III) is continuously electro-regenerated, the adsorbed urea molecule can be completely oxidized without any desorption of intermediates, contrary to the case with chemically synthesized particles, containing sacrificial NiOOH.

Once the partial orders known, the kinetic constant, noted $k_{E\chi}$, is deduced using the same method than in section §3.1.1. On the basis of eleven experiments carried out (see §SM. 6), $k_{E\chi}$ is found to vary in the range from $2.32\times10^{24}$ to $4.24\times10^{24}$ $mol^{-0.2}.\left(m_{elec}^2\right)^{-6}.(m^3)^{0.2}.s^{-1}$. The average value is equal to $2.86\times10^{24}$ $mol^{-0.2}.\left(m_{elec}^2\right)^{-6}.(m^3)^{0.2}.s^{-1}$ and used for the following calculations. Finally, the proposed kinetic law for the urea oxidation by the electrochemically generated nickel(III) sites can be written as the Eq. ( 27 ).

$$r_{E\chi} = (2.86 \pm 1.38) \times 10^{24} \times [CO(NH_2)_2]^{0.3} \times [OH^-]^{0.9} \times (S_{electrode})^5 \qquad (27)$$

### 3.3 Proposed mechanism for the urea complete electrooxidation

Based on the current state-of-art, Figure 4-a-b propose an overall mechanism for urea degradation involving electrochemically generated nickel(III) sites. The reaction scheme is composed of different pathways leading to the formation of by-products previously identified in the liquid phase[27].

The urea degradation mechanism from electrogenerated nickel(III) site can be classified into the nucleophilic oxidation reaction class[38,39] (as for the methanol oxidation on nickel(III)[40]), involving two pathways: successive *(i)* electrogenerated $Ni(OH)_2$ catalyst dehydrogenation reaction followed by *(ii)* a spontaneous nucleophilic dehydrogenation reaction. Firstly, the urea is adsorbed on a nickel(III) site[41], formed by the catalyst dehydrogenation reaction of nickel(II) oxidation. By analogy to the urease action on urea[42,43], a second active nickel(III) site is required to pursue the oxidation (step 2). Following the first nucleophilic attack onto a hydroxide group, two reactional pathways (step 3 and/or step 20) can be considered, favoring the formation of either ammonia (step 5), nitrite (steps 4, 8-19), and carbonate ions (steps 4-7), or cyanate ions (steps 20-22). The formation of ammonia and carbonate ions belongs to the same reactional pathway, thus suggesting an equimolar formation of these by-products over time. The nitrification route on nickel sites shown in Figure 4-b leads to the formation of nitrite. This route has been already studied by DFT[44], voltammetry and electrolyzes[45]. This latter route does not rule out the production of nitrogen during oxidation, even if several works[23,24,46] have reported the overoxidation of nitrogen into undesired NOx compounds at the expense of a nitrogen production. It should be noted that *(i)* the formation of cyanate (steps 21-22) and nitrite (steps 4, 18, 19) ions occurs in equimolar way, and *(ii)* most of the reactions constituting the proposed mechanism require hydroxide ions, and consequently directly decrease the local pH

at the electrode surface. This reaction scheme, reflects the complexity of a fully detailed kinetic approach that will requires a very large number of experiments so as to be able to determine each elementary kinetic constant (from $k_1$ to $k_{22}$, forward and backward).
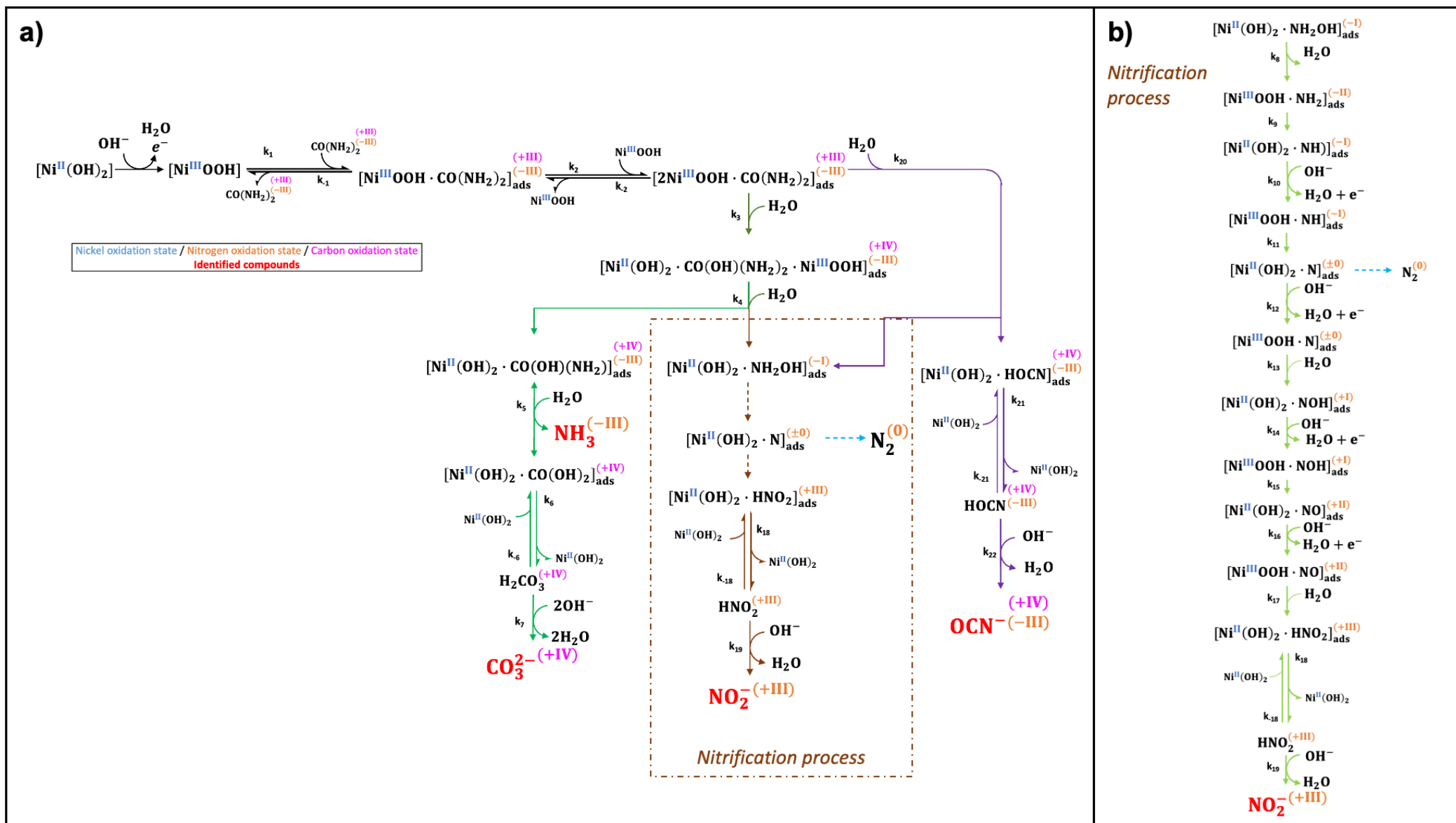
Figure 4 Proposed overall mechanism for UEO in alkaline media on a bare nickel anode covered after polarization by the system NiOOH/Ni(OH)$_2$. On the left side, a) the mechanism shows the main and side chemical pathways leading to N$_2$ and CO$_2$ (under CO$_3^{2-}$ form) as well as the by-products previously identified in the liquid phase[27] and b) detailed nitrification route.

# 4 Global modeling of the urea electro-oxidation

## 4.1 Establishment of the predictive model

Various potentiostatic electrolyzes with high conversions of urea have been performed in our previous work[27], for which the variations of the concentrations of urea and by-products with electrolyzes times have been determined and can be thus used to validate the model. The latter is based on the kinetic data obtained in the previous sections and involves all the physical processes occurring at the anode and in the bulk. Besides, the model is expected to be applicable at larger scale.

Let's consider that a one-dimensional description, depending on the distance to the electrode, is sufficient (for parallelepipedal electrochemical cells and planar anodes) to solve the mass transport phenomena coupled to the HCR in a porous catalytic layer. A schematic representation of the half-cell is given in Figure 5.
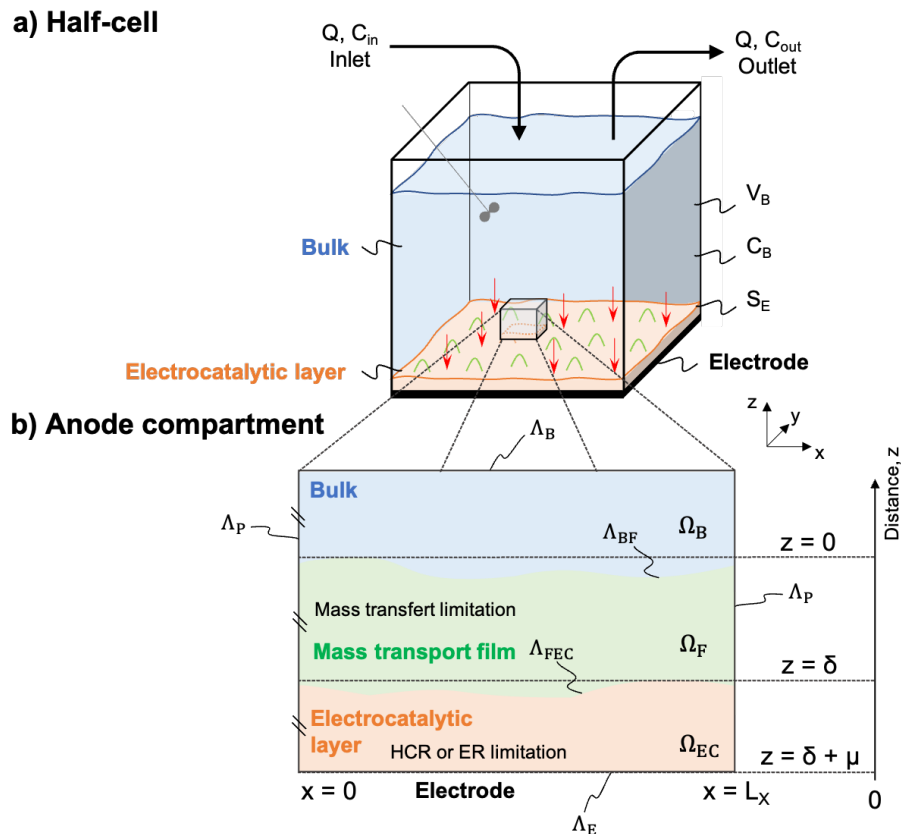


Figure 5 a) Schematic representation of the electrochemical half-cell. The large scale includes a perfectly stirred liquid phase and an electroactive layer of nickel oxide mixtures on the metal electrode surface. b) View of the various sensitive areas including possible limiting physical phenomena. The enlargement scheme contains three subdomains characterized by the occurrence of different phenomena: (1) a perfectly mixed zone, $\Omega_B$, that is

connected to the bulk liquid, (2) a mass transport boundary film $\Omega_F$, and (3) the matrix of the electrocatalytic nickel oxide layer $\Omega_{EC}$ at the electrode surface. Each boundary of the system is labeled by $\Lambda$. $\Lambda_{BF}$ represents the boundary between the bulk $\Omega_B$ and mass transport boundary film $\Omega_{EC}$ areas. $\Lambda_{FEC}$ represents the boundary between the film $\Omega_F$ and electrocatalytic film $\Omega_{EC}$ areas. $\Lambda_E$ and $\Lambda_B$ represent the massive electrode and wall boundaries of the system, respectively. (illustration adapted from Picioreanu et al.[47])

The aim is here to model the behavior of the electrochemical system during potentiostatic electrolyzes on a massive nickel electrode (supposed in equipotential conditions) of a stirred aqueous solution of urea in alkaline medium. During the electrode polarization, the following reactions will take place on the nickel compounds; starting by the Eq. ( 28 ) and followed by the Eq ( 1 ). At the applied electrolyzes potential (*i.e.* the one measured at the diffusion plateau of i-E curves, 0.55 V as illustrated in Figure 3), the reaction described in Eq. ( 28 ) occurs until the electrode is completely covered by Ni(OH)$_2$ layer. Then the catalytic cycle urea/NiOOH/Ni(OH)$_2$ occurs.

$$Ni + 2OH^- \rightarrow Ni(OH)_2 + 2e^- \tag{28}$$

### 4.1.1   Model assumptions

With the objective of building a robust model, it is necessary to formulate a clear framework and the appropriated assumptions:

*(i)*   Nickel(II) oxidation reaction occurs in a layer of a constant thickness µ which porosity ω, tortuosity τ and surface in contact with the solution remain unchanged throughout the electrolysis. Such assumption is supported by the fact that no significant release of nickel oxides has been measured by inductively coupled plasma (ICP) measurements performed at the end of each electrolysis (detection limit equals to 100 ppb). Porosity is evaluated considering that the nickel sites in the reactive layer are disposed as face-centered cubic unit cell with an atomic packing factor estimated at 0.74. Moreover, the tortuosity, τ, is estimated at $\pi/2$ as the ratio between the half-circumference of a sphere ($\pi \times r$) and the diameter of the sphere ($2 \times r$) (corresponding to the shortest path). The diffusion

coefficient in the reactive layer $(\delta < z < \delta + \mu)$ is then calculated as an effective diffusion coefficient $D_{i,w}^{eff}$ according to the Eq. ( 29 ).

$$D_{i,w}^{eff} = D_{i,w} \times \frac{\omega}{\tau} \qquad (29)$$

where $D_{i,w}$ is the diffusion binary coefficient of the specie i in the water ($m^2.s^{-1}$), $\omega$ the porosity of the layer of thickness $\mu$ (dimensionless) and $\tau$ the tortuosity (dimensionless). The values of the urea diffusion coefficient were previously calculated for different KOH concentrations, from the Stokes-Einstein equation[27].

*(ii)* The nickel oxides $Ni(OH)_2$ and $NiOOH$ are here considered as electronic conductors[48,49], making the electronic transfer invariant in the whole $\mu$ layer. On the other hand, most of the electrolyzes are performed under potentiostatic conditions. Since the applied potential is sufficiently anodic to allow (energetically speaking) the immediate conversion of any $Ni(OH)_2$ released from the HCR to $NiOOH$, one can assume that after a few minutes of electrolysis, the surface concentrations of $Ni(OH)_2$ and $NiOOH$ become constant and that the term related to the accumulation of these species is null. The geometry of the system is supposed to be independent of the length and width of the reactive layer and the radial diffusion to be negligible. Once formed, $NiOOH$ will react with urea and hydroxide ions according to Eq. ( 30 ).

$$\begin{aligned} r_{E\chi}(\delta \leq z \leq \delta + \mu, t) &= k_{E\chi} \times [OH^-]^{\beta_{E\chi}} \times (S_{elec})^{\gamma_{E\chi}} \times [CO(NH_2)_2]_{(\delta \leq z \leq \delta + \mu, t)}^{\alpha_{E\chi}} \\ &= k_{app} \times [CO(NH_2)_2]_{(\delta \leq z \leq \delta + \mu, t)}^{\alpha_{E\chi}} \end{aligned} \qquad (30)$$

where $k_{app}$ is the apparent constant ($mol^{1-\alpha_{E\chi}}.\left(m_{elec}^2\right)^{-1}.\left(m_{bulk}^3\right)^{\alpha_{E\chi}-1}.s^{-1}$).

It should be noted that the proposed kinetic equation does not take into account the consumptions of nickel peroxide and hydroxide ions during the chemical reactions leading to the products and by-products.

*(iii)* The concentration of urea and hydroxide ions in the layer µ is considered as a spatially continuous function; the nickel particles are assumed to be small enough not to impact the spatial concentration profile.

### *4.1.2   Governing equations: urea mass balances*

From these assumptions, the predictive model gives the urea concentration profile in all areas indicated in Figure 5. Into the bulk, the anolyte is assumed to be perfectly stirred, and the urea concentration is therefore considered uniform in the bulk volume, $\Omega_B$. The macroscopic balance of urea can be written as Eq. ( 31 ).

$$\text{Accumulation flux } + \text{ Diffusion flux } + (\text{Feed} + \text{Output})_{\text{flux in continuous reactor}} = 0$$

$$\begin{array}{c} \Omega_B \\ z \leq 0 \end{array} \quad V^{\text{bulk}} \times \frac{\partial [CO(NH_2)_2]_{z \leq 0}}{\partial t} + \left[ D_{\text{urea,w}} \times S_{\text{electrode}} \times \frac{\partial [CO(NH_2)_2]}{\partial z} \right]_{z=0} \quad (31)$$

$$+ Q \times ([CO(NH_2)_2]_{\text{Feed}} - [CO(NH_2)_2]_{\text{Output}}) = 0$$

where Q is the volumetric flow rate ($m^3.s^{-1}$).

In the present work, the results are obtained in a batch electrolyzer (Q = 0). Unlike in $\Omega_B$, the urea concentration in the diffusion film $\Omega_F$, is subject to spatial variation caused by the urea diffusion phenomenon due to the chemical reaction in $\Omega_{EC}$. The microscopic mass balance can be written as the Eq. ( 32 ).

$$\text{Accumulation flux } + \text{ Diffusion flux} = 0$$

$$\begin{array}{c} \Omega_F \\ 0 \leq z \leq \delta \end{array} \quad (S_{\text{electrode}} \times \delta) \times \left[ \frac{\partial [CO(NH_2)_2]}{\partial t} - \left[ D_{\text{urea,w}} \times \frac{\partial^2 [CO(NH_2)_2]}{\partial x^2} \right] \right] = 0 \quad (32)$$

In the $\Omega_{EC}$ area, the coupling of the HCR to the urea diffusion into the porous solid are the main occurring phenomena. The microscopic mass balance can be written according to the Eq. ( 33 ).

$$\text{Accumulation flux} + \text{Chemical reaction flux} + \text{Diffusion effective flux} = 0$$

$\Omega_{EC}$
$\delta \leq z \leq \delta + \mu$

$$(S_{electrode} \times \mu) \times \left[\frac{\partial[CO(NH_2)_2]}{\partial t} + S_{electrode} \times r_{E\chi}\right.$$

$$\left. - D_{urea,w}^{eff} \times \frac{\partial^2[CO(NH_2)_2]}{\partial x^2}\right] = 0$$

$$( 33 )$$

Eq. ( 33 ) represents a classical situation of a boundary value problem (shooting method) and its resolution is well documented in other works[50,51]. The resolution state of the model is a pseudo-steady state where the resolution is established by a succession of steady states, in the mass transport area as well as the electroactive layer, and a transient state in the bulk. The model resolution method is presented in see §SM. 7.

### 4.1.3   Boundary and initial conditions

The following initial and boundary conditions are applied:

*(i)*     At initial time, the urea concentration is assumed to be uniform throughout the whole system and equal to the initial concentration in the volume according to Eq. ( 34 ).

$\forall \Omega$
$t = 0$

$$C(z, 0) = C_{ini}$$

$$( 34 )$$

*(ii)*    It is considered that the urea does not directly react at the electrode neither with $Ni(OH)_2$ nor Ni; therefore, the mass flux arriving at the surface of the metal electrode $\Lambda_E$ and at both frontiers $\Lambda_P$ of the system, are assumed to zero according to Eq. ( 35 ).

$\forall \Lambda_E, \Lambda_P$
$\forall t$

$$\left.\frac{\partial[CO(NH_2)_2]}{\partial z}\right|_{z=\Lambda_E,\Lambda_P} = 0$$

$$( 35 )$$

*(iii)*   The continuity of the concentrations in each $\Omega$ domain, especially in the $\Omega_{EC}$ area, is ensured by the equality of the concentrations at each $\Lambda$ boundary of the system following the Eqs. ( 36 )-( 37 ) :

$$C_{\Omega_B,\Lambda_{BF}}(0,t) = C_{\Omega_F,\Lambda_{BF}}(0,t) \qquad (36)$$

$\forall t$

$$C_{\Omega_F,\Lambda_{FEC}}(\delta,t) = C_{\Omega_{EC},\Lambda_{FEC}}(\delta,t) \qquad (37)$$

Since the mass transport properties are significantly different in the domains $\Omega_F$ and $\Omega_{EC}$ (diffusion constant, thickness, concentration continuity), the equality of urea flux can be described as Eq. ( 38 ).

$$\forall t \qquad \frac{D_{urea,w}}{\delta} \times \left.\frac{\partial [CO(NH_2)_2]}{\partial z}\right|_{z=\Lambda_{FEC}}^{\Omega_F} = \frac{D_{urea,w}^{eff}}{\mu} \times \left.\frac{\partial [CO(NH_2)_2]}{\partial z}\right|_{z=\Lambda_{FEC}}^{\Omega_{EC}} \qquad (38)$$

These changes can be expressed according to a Biot dimensionless number as shown in Eq. ( 39 ).

$$Bi = \frac{k_{m,\Omega_F}}{k_{m,\Omega_{EC}}} = \frac{D_{urea,w}}{\delta} \times \frac{\mu}{D_{urea,w}^{eff}} \qquad (39)$$

where $k_m$ is the mass transport coefficient (m.s$^{-1}$).

### 4.2 Comparison between predictions and experimental data

#### *4.2.1 Thicknesses of the diffusion film and the electrocatalytic layer*

Two physical dimensions of the system need to be determined prior to the application of the model: the thickness of the diffusion layer, $\delta$, and the thickness of the electrocatalytic layer, $\mu$. Concerning the diffusion layer, the anodic oxidation limit current, observed on the urea diffusion plateau, is proportional to the concentration of the electroactive species. Here, nickel(III) is the electroactive specie, but its concentration will vary proportionally to that of urea according the catalytic cycle already mentioned in the previous section. Then, the following Eq. ( 40 ) can be applied.

$$\delta = \frac{n \times \mathcal{F} \times D_{urea,w} \times [CO(NH_2)_2]^{bulk}}{j_{plateau}^{\infty}} \qquad (40)$$

where $j_{plateau}^{\infty}$ is the limit current density current measured at the diffusion plateau in steady state ($A.m^{-2}$) at a potential varying in the range of 0.51 and 0.55 V (see Figure 3), n the number of exchanged electrons (dimensionless, 1 in case of nickel(II)/nickel(III)). Considering the values obtained in Figure 3-a for the lowest urea concentration (where the concentration of urea at the electrode is closed to 0, the molar flux arriving at the electrode becomes constant), a value of $\delta = (3.4 \pm 0.2) \times 10^{-5}$ m is determined.

The thickness of the electrocatalytic layer have been estimated in our previous study[27] and found equal to $\mu = (4.9 \pm 0.4) \times 10^{-8}$ m.


### 4.2.2 *Urea electrolysis on nickel electrode : case results and comparison*

In order to evaluate the veracity of the model, the urea concentrations experimentally measured in the bulk for various electrolyzes for which high conversions are achieved, will be considered and compared to the ones predicted by the model.
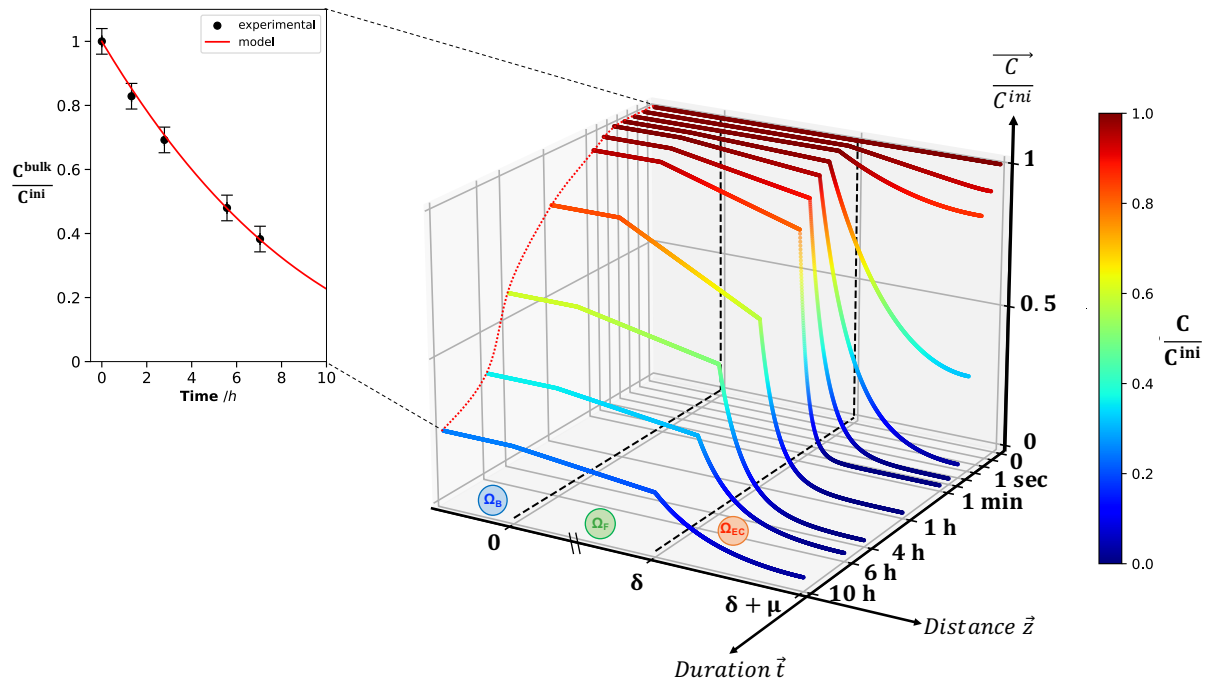
Figure 6 Spatio-temporal profiles of the urea concentration during a potentiostatic electrolysis at 0.55 V of a 0.33 mol.L$^{-1}$ urea solution in alkaline media (5 mol.L$^{-1}$ KOH), on nickel massive electrode. Inset: dimensionless urea concentrations in the bulk $\Omega_B$ measured experimentally (black filled circles) and predicted by the model (red line).

Figure 6 illustrates the spatio-temporal profiles of the urea concentration predicted by the model. The three spatial zones are quite distinct and well represented, allowing a good understanding of the involved processes ($\Omega_B$, $\Omega_F$: transport phenomena / $\Omega_{EC}$: transport phenomena and heterogeneous reaction). A non-linear time scale is represented for a better readability of the phenomena occurring.

In the reaction area $\Omega_{EC}$, the flux at the metal electrode (at $z = \delta+\mu$) equals to 0. The concentration in this $\Omega_{EC}$ zone starts to decrease according to a non-linear profile and tends towards a pseudo-steady state until the chemical regime competes with the diffusion flux from the diffusion film $\Omega_F$. A linear concentration profile in the $\Omega_F$ zone is thus obtained.

In the bulk area $\Omega_B$, the assumption of a perfectly stirred batch reactor is equivalent to an identical concentration at all points (at $z < 0$). The breaking slope observed at $z = \delta$ is representative of the urea fluxes transfer to the electrode. They indicate the discontinuities in the urea fluxes between the two media: liquid $\Omega_F$ and the catalytic $\Omega_{EC}$ layer of NiOOH/Ni(OH)$_2$. Both layers exhibit different mass transport properties (diffusion constant,

thickness, concentration continuity) according to the Biot number in Eq. ( 39 ). In the experimental conditions related to Figure 6, and at a KOH concentration of 5 mol.L$^{-1}$, this ratio between the mass transfer constants in the diffusion film and in the electrocatalytic layer, respectively, is estimated to be 112, thus reflecting a diffusional limitation in the porous zone compared to the diffusion film.

The inset in Figure 6 illustrates the simulated temporal evolution of the urea concentration in the bulk (continuous line), and a good agreement is observed with the experimental points obtained in our previous work[27].
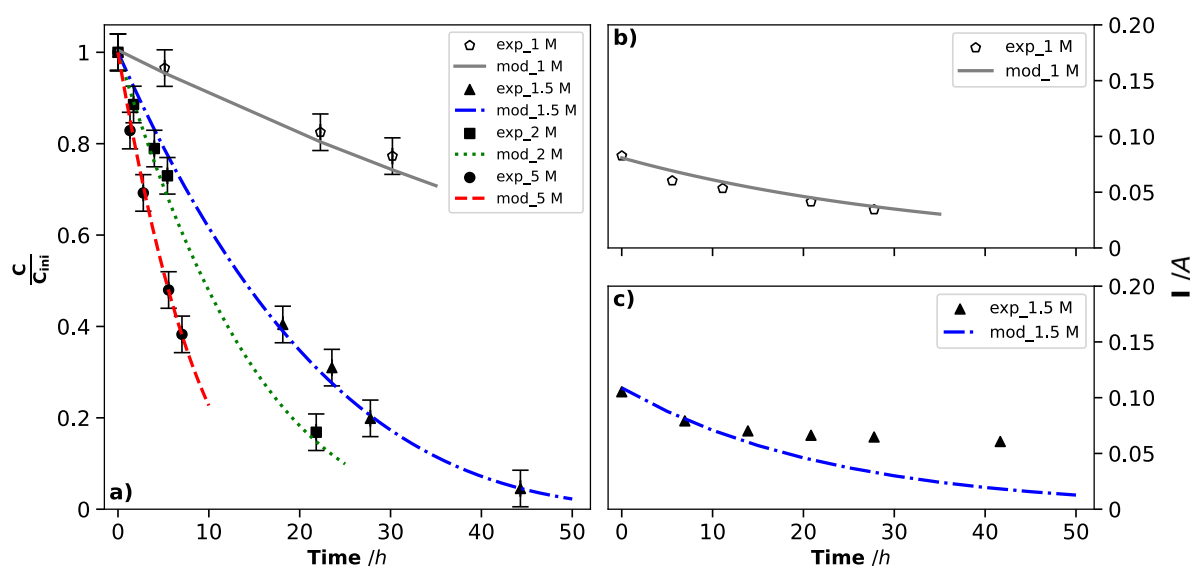


Figure 7 *Left:* a) Temporal variations of the normalized urea concentration in the bulk during potentiostatic electrolysis on nickel massive electrode in alkaline media. Experimental results are plotted for different KOH concentrations: 1 mol.L$^{-1}$ (◇), 1.5 mol.L$^{-1}$ (●), 2 mol.L$^{-1}$ (■) and 5 mol.L$^{-1}$ (▲). Filled symbols are obtained with an S/V ratio of 8 m$^{-1}$. The unfilled symbols are obtained with an S/V ratio equal to 20 m$^{-1}$. The lines represent the temporal profiles of the urea concentration predicted by the model at each KOH concentration.
*Right:* (b-c) Experimental and predicted profiles of the current intensity during electrolysis with a distance between electrodes of b) 15 cm using a H-type cell without separator and c) 3 cm using an undivided Metrohm® type-cell.

Figure 7-a compares the predicted (continuous line) and experimental (dots) normalized urea concentrations in the bulk, obtained during electrolyzes at different KOH concentrations, using two S/V ratios, where significant conversion rates of urea were reached. Data obtained at S/V ratio of 8 are extracted from our previous work[27]. In addition to examine the validity of the model on an enhanced value of S/V ratio, an alkaline electrolysis was carried out using an anode

surface of 26 cm$^2$ into 130 mL of electrolyte. A good agreement is observed between the experiments and the model since the maximum deviation of urea concentration is observed at 6 %.

An additional validation of the model is performed by comparing the temporal variation of the current predicted by the model according to Eq. ( 41 ) with the experimental one.

$$\text{Electrogenerated Ni}^{(\text{III})} \text{ flux } = 6 \times \text{ Urea chemically reacted flux}$$

$$
\begin{aligned}
I &= nFSV\nu_{\text{Ni(III)}} \int_{z=\delta}^{z=\delta+\mu} r_{E\chi}(z) \times dz \\
&= \left[ n\mathcal{F}V\nu_{\text{Ni(III)}} k_{E\chi} \times [OH^-]^{\beta_{E\chi}} \times (S_{\text{electrode}})^{\gamma_{E\chi}+1} \right] \\
&\quad \times \int_{z=\delta}^{z=\delta+\mu} [CO(NH_2)_2]^{\alpha_{E\chi}} \times dz
\end{aligned}
\qquad (\,41\,)
$$

As shown in Figure 7-b, the model predicts the current with a maximum deviation of 4 %, thus implying that the main assumption considering a constant temporal superficial concentration of nickel(III) would be verified.

Results of electrolysis indicated in Figure 7-c were obtained using an undivided Metrohm$^{®}$ type cell, containing a strongly stirred (1000 RPM) solution. In these conditions, the electrogenerated hydrogen at the cathode (diameter < 1 mm) dispersed in the bulk, and consequently in the immediate environment of the anode. Strong dispersion of gaseous $H_2$ increase the gas/liquid interface and facilitates its dissolution (the stationary concentration of hydrogen can achieve its solubility). Under the applied anodic potential (0.55 V), the dissolved hydrogen can be oxidized, and in these conditions the observed current is composed by:

*(i)* the urea oxidation current (temporally decreasing);

*(ii)* the hydrogen oxidation current[52–54] induced by the reaction Eq. ( 42 ), first increasing until the steady state is reached, *i.e* a constant gaseous $H_2$ flux arrived at the anode area.

$$H_2 + 2OH^- \rightarrow 2H_2O + 2e^- \qquad\qquad (\,42\,)$$
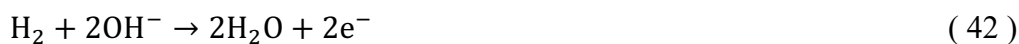
These facts explain the observed difference of the current between the model and the experimental data, which varies from 1 to 80 %. Note that, this difference will decrease as a function of time. Indeed, as the urea concentration is depleted, the corresponding fraction of anodic current is decreased, thus implying the overall current to decreases. In these conditions the hydrogen electrogenerated flux at the cathode decreases.

As the hydrogen is not maintained in the reactor, its contribution to the anode current will also decrease until to be cancelled (simultaneously to urea). The difference in current intensity between the theoretical and experimental data corresponds to the current 'lost' due to the absence of a physical separator.

## 5    Conclusions

This work allowed to highlight and characterize the kinetics of urea indirect electro-oxidation on active nickel(III) sites in alkaline medium. NiOOH particles, synthesized from commercial Ni(OH)$_2$ powder using NaOCl, were characterized by SEM, BET, XRD and particle size analysis. They exhibited spherical shape and their content in nickel(III) reached 80 %. Compared to Ni(OH)$_2$ solids, the crystallinity of the synthesized NiOOH particles appears to be much lower than that of the starting powder, reflecting a core-shell geometry. The particles after synthesis, were composed of an amorphous NiOOH shell and a Ni(OH)$_2$ core.

Firstly, the kinetic study was performed using chemically synthesized nickel(III) particles. By using the method of initial rate of OH$^-$ disappearance, the partial reaction order of urea was evaluated at 0.3, highlighting a limitation of the urea adsorption on the active sites of nickel. Subsequently, the partial orders of 0.6 and 1.9, respectively attributed to hydroxide ions and nickel active sites, were determined using the same type of experimental measurements. The dependence of the kinetic rate on hydroxide ions appeared to be low, whereas it was higher on

nickel ($\gamma_\chi \approx 2$). Although more experiments would be required to precisely identify the reaction mechanism, an order of 2 against the nickel(III) suggesting that urea would bind to two nickel sites either *(i)* via both amine groups or *(ii)* via one of the amine groups and the ketone group. Besides, this low dependence of the kinetic rate to dissolved species concentrations would suggest possible mass transport limitations in the solid spherical particles; indeed, after a consumption of nickel(III), the transformed urea or even the by-products must desorb, and find another nickel(III) available to absorb, to pursue the oxidative process. Moreover, the performed BET analysis showed particles having low specific surface area ($8.51 \ m^2.g^{-1}$) , which would tend to incriminate limitation by the mass transport into the particles. This initial kinetic law did not consider the effect of the urea oxidized intermediates on $OH^-$ or nickel(III) consumption, as their initial concentration was close to zero. Since the limitation of the overall process, at least initially, appears to be due to the adsorption, these intermediates do not accumulate; they rapidly convert to observed products, and therefore do not affect the kinetic rate. This fact was validated by the integration as a function of time, of the initial kinetic law *i.e.* for higher conversion rates. The obtained theoretical variation of the $OH^-$ concentration was successfully compared with the experimental one (maximum deviation of 6 %).

Secondly, the kinetics of indirect electro-oxidation of urea was studied by polarizing a massive nickel electrode which enabled the formation of a catalytic layer $NiOOH/Ni(OH)_2$, and thus ensured the urea oxidation thanks to the electrochemical continuous regeneration of the nickel(III) actives sites. Under these assumptions, the kinetic rate law showed a partial order of urea close to the previous value (*i.e.* 0.3). However, the order of the nickel surface was found to be high ($\gamma_{E\chi} \approx 5$), signifying that the adsorption of urea onto nickel(III) sites was followed by complete oxidation of this urea by five nickel(III) generated electrochemically, almost instantaneously due to potentiostatic polarization of the anode at the required potential.

Coupled with the previously performed mass balances carried out our preparative electrolyzes (which demonstrated the presence of various by-products in the liquid phase), the present kinetic study made possible to build up a relatively complete multi-pathway (22 sequential steps, four different ways and 5 urea oxidation products) mechanism able to describe the process of indirect electro-oxidation of urea.

Finally, this kinetic study was implemented into a more general predictive model combining *(i)* mass transport phenomena, in a liquid film and in a solid porous catalytic layer with *(ii)* the indirect electrocatalytic chemical reaction occurring in the previous layer, and finally *(iii)* assisted by the quasi-instantaneous regeneration of the reaction driving factor *i.e.* the nickel(III) catalytic sites. The resolution of the established model on the basis of the shooting method allowed to predict spatio-temporal urea concentration profiles for various operating conditions. These predicted results were compared to the experimental ones for different hydroxide concentrations and S/V ratio. A satisfactory agreement was observed with low (< 5 %) deviations, thus opening interesting perspectives for further larger-scale operations in the urea mineralization.

**Notation**

*Letters*

- CE: counter electrode

- E: applied potential (mV *vs.* Hg/HgO)
- ER: electrogenerated reaction
- $\mathcal{F}$: Faraday's constant (96 500 C.mol$^{-1}$)
- I: current (A)
- j: current density (A.m$^{-2}$)
- HCR: heterocatalytic chemical reaction
- n: number of exchanged electron (dimensionless)
- Q: flowrate (m$^3$.s$^{-1}$)
- t: time (s)
- T: temperature (K)
- UEO : urea electro-oxidation
- V, V$_B$: suspension volume / electrolyte volume (m$^3$)
- WE: working electrode
- x: length of the electrode (m)
- X: conversion rate (dimensionless)
- z: distance to the electrode (m)
- δ: diffusion layer thickness (m)
- ε: nickel accessibility factor (dimensionless)
- μ: mixed oxides layer length (m)
- τ: tortuosity of the electrocatalytic layer (dimensionless)
- ω: porosity of electrocatalytic layer (dimensionless)
- θ: scattering angle (°)
- ξ: extent of reaction (mol)

*Subscripts*

- $d_{10}$, $d_{50}$, $d_{90}$: percentile value diameters (μm)
- $d_{32}$, $d_{43}$: Sauter Mean diameter and De Brouckere Mean diameter (μm)
- $D_{i,w}$: diffusion binary coefficient of the specie i in the water (m$^2$.s$^{-1}$)
- $D_{i,w}^{eff}$: effective diffusion binary coefficient of the specie i in the water in porous media (m$^2$.s$^{-1}$)
- $I_{plateau}$: limiting current, observed at the plateau signal (A)
- $I_{plateau}^{\infty}$: limiting current, observed at the plateau signal in steady state (A)

- $j_{plateau}^{\infty}$: limiting density current, observed at the plateau signal in steady state ($A.m^{-2}$)

- $k_{app}, k'_{app}, k''_{app}$: apparent constants of $r_\chi(t)$ (variable unit)

- $k_m$: mass transport coefficient ($m.s^{-1}$)

- $k_\chi$: reaction rate constant of $r_\chi$ ($mol^{1-\alpha_\chi-\beta_\chi-\gamma_\chi}.m^{3(\alpha_\chi+\beta_\chi)-3}.(g_{cat}.s)^{-1}$)

- $k_{E\chi}$: reaction rate constant of $r_{E\chi}$ ($mol^{1-\alpha_{E\chi}-\beta_{E\chi}-\gamma_{E\chi}}.m^{3(\alpha_{E\chi}+\beta_{E\chi})-2}.s^{-1}$)

- $m_{cat}$: mass of powder (g)

- $M_{Ni^{III}}$: NiOOH molar mass ($g.mol^{-1}$)

- $n_i$: amount of substance i (mol)

- $r_\chi$: instantaneous reaction rate for powder nickel(III) study ($mol.m^3.(g_{cat}.s)^{-1}$)

- $r_\chi^0$: initial rate of $r_\chi$ ($mol.m^3.(g_{cat}.s)^{-1}$)

- $r_{E\chi}$: kinetic law obtained on electrogenerated nickel(III) sites ($mol.m^2_{electrode}.s^{-1}$)

- $S_{electrode}$: electrode surface ($m^2$)

- $\alpha_\chi, \beta_\chi, \gamma_\chi$: partial orders of urea, hydroxide, and nickel respectively (dimensionless) determined with nickel-oxides synthesized powders

- $\alpha_{E\chi}, \beta_{E\chi}, \gamma_{E\chi}$: partial orders of urea, hydroxide, and nickel respectively (dimensionless) determined with nickel-oxides electrodes

- $\Gamma_i$: superficial concentration of the nickel at the oxidation state i ($mol.m^{-2}$)

- $\Lambda_i$: model border i

- $\rho_{cat}$: mass concentration of nickel(III) per unit of volume ($g_{cat}.m^{-3}$)

- $\Omega_B, \Omega_F, \Omega_{EC}$: model domains respectively, bulk, diffusion film and electrocatalytic layer

- $\nu_i$: stochiometric number of the reactant i (dimensionless)

- $\nu_{scan}$: potential scan rate ($V.s^{-1}$)

*Superscripts*

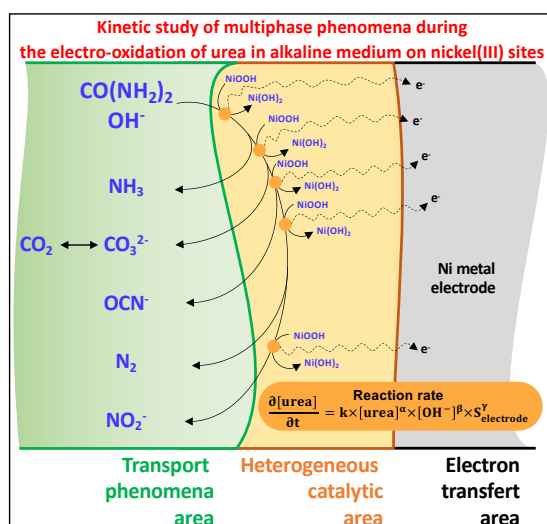- $C^{bulk}$: bulk urea concentration ($mol.m^{-3}$)

- $C^{electrode}$: electrode urea concentration ($mol.m^{-3}$)

- $C^F$: urea concentration at the interface between diffusion film and electrocatalytic layer ($mol.m^{-3}$)

## Plain Language Summary

The study presents kinetic and mechanistic approaches used as tools for the building of a predictive model enabling the optimization of the urea catalytic oxidation by active nickel sites, simultaneously to the hydrogen cathodic production.

## Graphical abstract



**Kinetic study of multiphase phenomena during the electro-oxidation of urea in alkaline medium on nickel(III) sites**

$$\frac{\partial[urea]}{\partial t} = k \times [urea]^{\alpha} \times [OH^-]^{\beta} \times S_{electrode}^{\gamma}$$

Reaction rate

Transport phenomena area — Heterogeneous catalytic area — Electron transfert area

Ni metal electrode

## References

1. Qadir M, Drechsel P, Jiménez Cisneros B, et al. Global and regional potential of wastewater as a water, nutrient and energy source. *Natural Resources Forum*. Published online 2020. doi:10.1111/1477-8947.12187

2. Bouatra S, Aziat F, Mandal R, et al. The Human Urine Metabolome. Dzeja P, ed. *PLoS ONE*. Published online 2013. doi:10.1371/journal.pone.0073076

3. Larsen TA, Gujer W. Separate management of anthropogenic nutrient solutions (human urine). *Water Science and Technology*. Published online 1996. doi:10.2166/wst.1996.0420

4. Boggs BK, King RL, Botte GG. Urea electrolysis: direct hydrogen production from urine. *Chemical Communications*. Published online 2009. doi:10.1039/b905974a

5. Kim J, Choi WJK, Choi J, Hoffmann MR, Park H. Electrolysis of urea and urine for solar hydrogen. *Catalysis Today*. Published online 2013. doi:10.1016/j.cattod.2012.02.009

6.      King RL, Botte GG. Investigation of multi-metal catalysts for stable hydrogen production via urea electrolysis. *Journal of Power Sources*. Published online 2011. doi:10.1016/j.jpowsour.2011.06.079

7.      Amstutz V, Katsaounis A, Kapalka A, Comninellis C, Udert KM. Effects of carbonate on the electrolytic removal of ammonia and urea from urine with thermally prepared IrO2 electrodes. *J Appl Electrochem*. 2012;42(9):787-795. doi:10.1007/s10800-012-0444-y

8.      Santoro C, Garcia MJS, Walter XA, et al. Urine in Bioelectrochemical Systems: An Overall Review. *ChemElectroChem*. Published online 2020. doi:10.1002/celc.201901995

9.      Kim OH, Choi HJ, Kang SY, et al. Towards outstanding performance of direct urea fuel cells through optimization of anode catalyst layer and operating conditions. *Journal of Electroanalytical Chemistry*. Published online 2022. doi:10.1016/j.jelechem.2022.116661

10.     Basumatary P, Konwar D, Yoon YS. A novel Ni Cu/ZnO@MWCNT anode employed in urea fuel cell to attain superior performances. *Electrochimica Acta*. Published online 2018. doi:10.1016/j.electacta.2017.12.123

11.     Ye K, Wang G, Cao D, Wang G. Recent Advances in the Electro-Oxidation of Urea for Direct Urea Fuel Cell and Urea Electrolysis. *Topics in Current Chemistry*. Published online 2018. doi:10.1007/s41061-018-0219-y

12.     Lan R, Tao S, Irvine JTS. A direct urea fuel cell – power from fertiliser and waste. *Energy & Environmental Science*. Published online 2010. doi:10.1039/b924786f

13.     Sayed ET, Eisa T, Mohamed HO, et al. Direct urea fuel cells: Challenges and opportunities. *Journal of Power Sources*. Published online 2019. doi:10.1016/j.jpowsour.2018.12.024

14.     Zhu B, Liang Z, Zou R. Designing Advanced Catalysts for Energy Conversion Based on Urea Oxidation Reaction. *Small*. Published online 2020. doi:10.1002/smll.201906133

15.     Sun X, Ding R. Recent progress with electrocatalysts for urea electrolysis in alkaline

media for energy-saving hydrogen production. *Catalysis Science & Technology*. Published online 2020. doi:10.1039/C9CY02618E

16. Ye K, Zhang D, Guo F, Cheng K, Wang G, Cao D. Highly porous nickel@carbon sponge as a novel type of three-dimensional anode with low cost for high catalytic performance of urea electro-oxidation in alkaline medium. *Journal of Power Sources*. Published online 2015. doi:10.1016/j.jpowsour.2015.02.149

17. Ding R, Qi L, Jia M, Wang H. Facile synthesis of mesoporous spinel $NiCo_2O_4$ efficient electrocatalysts for urea electro-oxidation. *Nanoscale*. Published online 2014. doi:10.1039/C3NR05359H

18. Li J, Wang S, Chang J, Feng L. A review of Ni based powder catalyst for urea oxidation in assisting water splitting reaction. *Advanced Powder Materials*. Published online 2022. doi:10.1016/j.apmate.2022.01.003

19. Yan W, Wang D, Botte GG. Nickel and cobalt bimetallic hydroxide catalysts for urea electro-oxidation. *Electrochimica Acta*. Published online 2012. doi:10.1016/j.electacta.2011.11.044

20. Vedharathinam V, Botte GG. Direct evidence of the mechanism for the electro-oxidation of urea on $Ni(OH)_2$ catalyst in alkaline medium. *Electrochimica Acta*. Published online 2013. doi:10.1016/j.electacta.2013.06.137

21. Daramola DA, Singh D, Botte GG. Dissociation Rates of Urea in the Presence of NiOOH Catalyst: A DFT Analysis. *The Journal of Physical Chemistry*. Published online 2010. doi:10.1021/jp105159t

22. Chakrabarty S, Offen-Polak I, Burshtein TY, Farber EM, Kornblum L, Eisenberg D. Urea oxidation electrocatalysis on nickel hydroxide: the role of disorder. *Journal of Solid State Electrochemistry*. Published online 2020. doi:10.1007/s10008-020-04744-6

23. Li J, Li J, Liu T, et al. Deciphering and Suppressing Over-Oxidized Nitrogen in Nickel-

Catalyzed Urea Electrolysis. *Angewandte Chemie International Edition*. Published online 2021. doi:10.1002/anie.202107886

24. Tatarchuk SW, Medvedev JJ, Li F, Tobolovskaya Y, Klinkova A. Nickel-Catalyzed Urea Electrolysis: From Nitrite and Cyanate as Major Products to Nitrogen Evolution. *Angewandte Chemie*. Published online 2022. doi:10.1002/ange.202209839

25. Vedharathinam V, Botte GG. Understanding the electro-catalytic oxidation mechanism of urea on nickel electrodes in alkaline medium. *Electrochimica Acta*. Published online 2012. doi:10.1016/j.electacta.2012.07.007

26. Singh RK, Schechter A. Electrochemical investigation of urea oxidation reaction on β-Ni(OH)$_2$ and Ni/Ni(OH)$_2$. *Electrochimica Acta*. Published online 2018. doi:10.1016/j.electacta.2018.05.049

27. Hopsort G, Pereira Do Carmo D, Latapie L, Loubière K, Groenen Serrano K, Tzedakis T. Progress toward a better understanding of the urea oxidation by electromediation of Ni(II)/Ni(III) system in alkaline media. *Electrochimica Acta*. Published online To be published (under revision).

28. Pan J, Sun Y, Wan P, Wang Z, Liu X. Synthesis, characterization and electrochemical performance of battery grade NiOOH. *Electrochemistry Communications*. Published online 2005. doi:10.1016/j.elecom.2005.05.004

29. Thimmasandra Narayan R. Effect of Crystallinity of β- and βbc-Nickel Hydroxide Samples on Chemical Cycling. Kalyanaraman R, ed. *Indian Journal of Materials Science*. Published online 2015. doi:10.1155/2015/820193

30. Shangguan E, Chang Z, Tang H, Yuan X, Wang H. Preparation of nickel oxyhydroxide by a new electrolysis method using spherical β-Ni(OH)$_2$. *International Journal of Hydrogen Energy*. Published online 2010. doi:10.1016/j.ijhydene.2010.01.098

31. Kashani Motlagh MM, Youzbashi AA, Hashemzadeh F, Sabaghzadeh L. Structural

properties of nickel hydroxide/oxyhydroxide and oxide nanoparticles obtained by microwave-assisted oxidation technique. *Powder Technology*. Published online 2013. doi:10.1016/j.powtec.2012.12.047

32.  Bantignies JL, Deabate S, Righi A, et al. New Insight into the Vibrational Behavior of Nickel Hydroxide and Oxyhydroxide Using Inelastic Neutron Scattering, Far/Mid-Infrared and Raman Spectroscopies. *The Journal of Physical Chemistry C*. Published online 2008. doi:10.1021/jp075819e

33.  Hall DS, Lockwood DJ, Bock C, MacDougall BR. Nickel hydroxides and related materials: a review of their structures, synthesis and properties. *Proceedings of the Royal Society A: Mathematical, Physical and Engineering Sciences*. Published online 2015. doi:10.1098/rspa.2014.0792

34.  Fu XZ, Zhu YJ, Xu QC, et al. Nickel oxyhydroxides with various oxidation states prepared by chemical oxidation of spherical $\beta$-Ni(OH)$_2$. *Solid State Ionics*. Published online 2007. doi:10.1016/j.ssi.2007.04.011

35.  Pardue HL. Kinetic aspects of analytical chemistry. *Analytica Chimica Acta*. 1989;216. doi:10.1016/S0003-2670(00)82005-X

36.  Casado J, Lopez-Quintela MA, Lorenzo-Barral FM. The initial rate method in chemical kinetics: Evaluation and experimental illustration. *Journal of Chemical Education*. Published online 1986. doi:10.1021/ed063p450

37.  Thomas LC, Dorizas A, Mech E. Comparison of Integration Vs. Fixed-Time Methods For Kinetic Analyses. *Analytical Letters*. Published online 1989. doi:10.1080/00032718908051382

38.  Chen W, Xie C, Wang Y, et al. Activity Origins and Design Principles of Nickel-Based Catalysts for Nucleophile Electrooxidation. *Chem*. Published online 2020. doi:10.1016/j.chempr.2020.07.022

39.      Chen W, Wang Y, Wu B, et al. Activated Ni-OH Bond in Catalyst Facilitates Nucleophile Oxidation Reaction. *Advanced Materials*. Published online 2022. doi:10.1002/adma.202105320

40.      Qi Y, Zhang Y, Yang L, et al. Insights into the activity of nickel boride/nickel heterostructures for efficient methanol electrooxidation. *Nature Communications*. Published online 2022. doi:10.1038/s41467-022-32443-5

41.      Ge J, Liu Z, Guan M, et al. Investigation of the electrocatalytic mechanisms of urea oxidation reaction on the surface of transition metal oxides. *Journal of Colloid and Interface Science*. Published online 2022. doi:10.1016/j.jcis.2022.03.152

42.      Mazzei L, Musiani F, Ciurli S. The structure-based reaction mechanism of urease, a nickel dependent enzyme: tale of a long debate. *JBIC Journal of Biological Inorganic Chemistry*. Published online 2020. doi:10.1007/s00775-020-01808-w

43.      Mazzei L, Cianci M, Benini S, Ciurli S. The Structure of the Elusive Urease–Urea Complex Unveils the Mechanism of a Paradigmatic Nickel-Dependent Enzyme. *Angewandte Chemie International Edition*. Published online 2019. doi:10.1002/anie.201903565

44.      Choueiri RM, Tatarchuk SW, Klinkova A, Chen LD. Mechanism of ammonia oxidation to dinitrogen, nitrite, and nitrate on β-Ni(OH)$_2$ from first-principles simulations. *Electrochemical Science Advances*. Published online 2021. doi:10.1002/elsa.202100142

45.      Shih YJ, Huang YH, Huang CP. Electrocatalytic ammonia oxidation over a nickel foam electrode: Role of Ni(OH)$_{2(s)}$- NiOOH$_{(s)}$ nanocatalysts. *Electrochimica Acta*. Published online 2018. doi:10.1016/j.electacta.2018.01.045

46.      Medvedev JJ, Tobolovskaya Y, Medvedeva XV, Tatarchuk SW, Li F, Klinkova A. Pathways of ammonia electrooxidation on nickel hydroxide anodes and an alternative route towards recycled fertilizers. *Green Chemistry*. Published online 2022. doi:10.1039/D1GC04140A

47.     Picioreanu C, Head IM, Katuri KP, van Loosdrecht MCM, Scott K. A computational model for biofilm-based microbial fuel cells. *Water Research*. Published online 2007. doi:10.1016/j.watres.2007.04.009

48.     Xiong X, Ding D, Chen D, et al. Three-dimensional ultrathin $Ni(OH)_2$ nanosheets grown on nickel foam for high-performance supercapacitors. *Nano Energy*. Published online 2015. doi:10.1016/j.nanoen.2014.10.029

49.     Li L, Xu J, Lei J, et al. A one-step, cost-effective green method to in situ fabricate $Ni(OH)_2$ hexagonal platelets on Ni foam as binder-free supercapacitor electrode materials. *Journal of Materials Chemistry A*. Published online 2015. doi:10.1039/C4TA05156D

50.     Lee J, Kim DH. An improved shooting method for computation of effectiveness factors in porous catalysts. *Chemical Engineering Science*. Published online 2005. doi:10.1016/j.ces.2005.05.027

51.     Natesan S, Ramanujam N. 'Shooting method' for singularly perturbed one-dimensional reaction-diffusion neumann problems. *International Journal of Computer Mathematics*. Published online 1999. doi:10.1080/00207169908804861

52.     Davydova ES, Speck FD, Paul MTY, Dekel DR, Cherevko S. Stability Limits of Ni-Based Hydrogen Oxidation Electrocatalysts for Anion Exchange Membrane Fuel Cells. *ACS Catalysis*. Published online 2019. doi:10.1021/acscatal.9b01582

53.     Zhou Z, Liu Y, Zhang J, Pang H, Zhu G. Non-precious nickel-based catalysts for hydrogen oxidation reaction in alkaline electrolyte. *Electrochemistry Communications*. Published online 2020. doi:10.1016/j.elecom.2020.106871

54.     Trinke P, Haug P, Brauns J, Bensmann B, Hanke-Rauschenbach R, Turek T. Hydrogen Crossover in PEM and Alkaline Water Electrolysis: Mechanisms, Direct Comparison and Mitigation Strategies. *Journal of The Electrochemical Society*. Published online 2018. doi:10.1149/2.0541807jes

**CRediT author statement**

*G. Hopsort:* Conceptualization, Data curation, Formal analysis, Investigation, Methodology, Validation, Visualization, Writing - original draft / *L. Latapie:* Conceptualization, Formal analysis, Investigation, Methodology, Resources / *K. Groenen Serrano:* Conceptualization, Formal analysis, Investigation, Supervision, Validation, Writing - review & editing / *K. Loubière:* Conceptualization, Formal analysis, Investigation, Supervision, Validation, Writing - review & editing / *T. Tzedakis:* Conceptualization, Formal analysis, Funding acquisition, Investigation, Methodology, Project administration, Supervision, Validation, Writing - review & editing.